DEVELOPMENTAL BIOLOGY

Time-series single-cell transcriptomics reveals pervasive daily rhythmicity and nocturnal spermatogenesis in the zebrafish testis

Taole Liu[1,2,3,4], Lianxin Wu[2,3], Shital Kumar Mishra[2,3], Qi Fang[1], Han Wang[1,2,3,4]*

The vertebrate testis has long been regarded as lacking strong cellular daily rhythmicity. Here, we use time-series single-cell RNA sequencing to construct a temporal atlas of the adult zebrafish testis. We identify previously unknown cell-type–specific markers and previously unidentified testicular subtypes and reveal that Sertoli cells, spermatogonia, and spermatids exhibit robust oscillations in key circadian clock genes. In contrast, Leydig cells and spermatocytes primarily exhibit rhythmic expression of key functional genes. We show that intercellular communication networks also exhibit daily rhythmicity. Pseudotime trajectory analysis demonstrates a notable nocturnal preference for germ cell progression. Disrupting circadian input via constant light reduced germ cell numbers and impaired fertility. Genetic ablation of *clock1a* arrests spermatogonial differentiation, whereas mutation of the rhythmic spermatocyte gene *hmgb1a* substantially reduces meiotic cells. Together, our findings redefine the testis as a highly rhythmic organ in which a precisely timed, nocturnally coordinated cellular symphony drives spermatogenesis.

INTRODUCTION

The vertebrate testis is a complex organ responsible for sperm production and hormone synthesis, comprising multiple types of germ and somatic cells (*1*, *2*). For decades, the testis has been considered an organ lacking significant circadian rhythmicity, as whole-organ studies failed to detect self-sustained oscillations of key circadian clock genes (*3*–*5*). Until recently, our work has revealed that Sertoli cells have a functional circadian clock critical for synchronizing spermatogenesis and promoting fertilization in zebrafish and mice (*6*). However, the extent of daily rhythmicity across distinct testicular cell types and how such rhythms temporally coordinate the complex process of spermatogenesis remain poorly understood (*7*–*9*).

Spermatogenesis is a highly coordinated process driven by systemic hormones and local paracrine factors within the spermatogonial niche (*10*–*12*). Initially, self-renewing spermatogonial stem cells, residing in the niche, are coordinated to divide in mitosis and then differentiate to produce successive meiotic spermatocytes, which then undergo continuous waves of gametogenesis during the reproductive period in adults (*13*–*15*). In vertebrates, the testis develops as a cyst unit in zebrafish, whereas it develops noncystically in mammals (*2*). In the cystic type of spermatogenesis in zebrafish, a group of developing germ cells, enveloped by Sertoli cells, synchronously forms a germ cell clone; and germ cells in the inner cyst, as a clone, or in the intercyst at different stages are well organized and synchronized in a temporal order (*2*). This inherent synchrony within cystic clones, combined with robust light-entrainable circadian clocks (*6*, *16*), makes zebrafish an ideal model for dissecting the temporal regulation of spermatogenesis at single-cell resolution.

Single-cell RNA sequencing (scRNA-seq) has revolutionized our understanding of testicular cell compositions and lineages (*17*–*20*). However, a critical limitation of previous scRNA-seq studies is their reliance on static snapshots from random time points, which inevitably masks dynamic temporal programs and may lead to misrepresentation of cell population ratios or even failure to detect transient cell states. Furthermore, discrepancies in cell-type annotation across species, such as the reported absence of testicular macrophages in zebrafish (*21*), may arise from such nontemporal sampling. Therefore, a systematic, time-resolved investigation at single-cell resolution is essential to decode the temporal logic governing testicular cellular interactions and fate decisions.

In this study, we perform a time-series scRNA-seq analysis of adult zebrafish testes at zeitgeber time (ZT) 1, 7, 13, and 19 over a 24-hour cycle. We aim to generate a temporal atlas of testicular cell types and identify previously unreported testicular markers and subtypes to determine the extent of daily rhythmicity across all somatic and germ cells, to elucidate the daily timing of germ cell differentiation transitions using pseudotime trajectory analysis, and to investigate whether intercellular communication networks exhibit coordinated daily variations.

RESULTS

Time-series scRNA-seq analysis generates a temporal atlas of zebrafish testicular cell clusters

Time-series bulk RNA-seq analyses have recently revealed that the testes exhibit robust rhythmicity in multiple signaling pathways and cellular physiological processes in zebrafish, mice (*6*), and baboons (*22*). In particular, the Sertoli cells display robust circadian rhythmicity (*6*). However, it is still unknown whether daily rhythmicity exists in other testicular cell types. We conducted time-series scRNA-seq analysis of testes collected from adult zebrafish at 6-hour intervals over a consecutive 24-hour period to investigate daily rhythmicity at the cellular and molecular levels in the zebrafish testis (Fig. 1A).

The four datasets of these 29,315 cells collected over 1 day were first merged, with cell counts of 6705 at ZT1, 7691 at ZT7, 7202 at ZT13, and 7537 at ZT19 (Fig. 1B), and annotated with previously reported markers in the testis (*20*, *23*). Six testicular cell clusters were identified by dimensional reduction, including somatic cells

[1]Department of Neurology, The First Affiliated Hospital of Soochow University, Suzhou, Jiangsu 215006, China. [2]Center for Circadian Clocks, Soochow University, Suzhou, Jiangsu 215123, China. [3]Jiangsu Key Laboratory of Drug Discovery and Translational Research for Brain Diseases, School of Basic Medical Sciences, Suzhou Medical College, Soochow University, Suzhou, Jiangsu 215123, China. [4]Biomedical Basic Research Center (BBRC) of Jiangsu, Suzhou Medical College, Soochow University, Suzhou, Jiangsu 215123, China.
*Corresponding author. Email: han.wang88@gmail.com, wanghan@suda.edu.cn

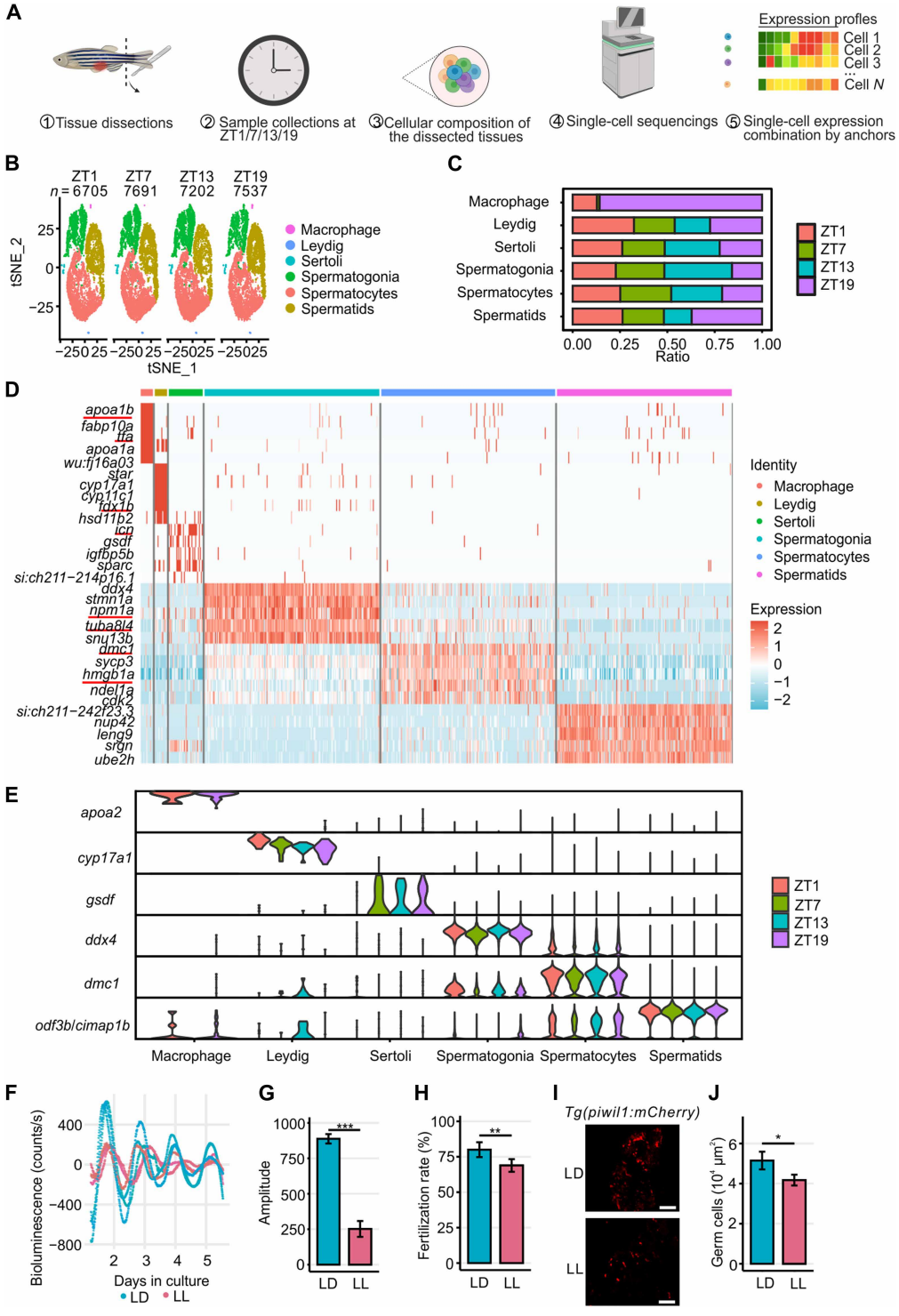

Fig. 1. Time-series single-cell RNA-seq analysis of adult zebrafish testis. (**A**) Diagram of experimental procedures for testis sampling and subsequent scRNA-seq analysis. The zebrafish testes were collected every 6 hours for consecutive 24 hours. Created in BioRender. Liu, T. (2026) https://BioRender.com/sab5066 (**B**) t-distributed stochastic neighbor embedding (tSNE) dimensional reduction of the data of 29,315 cells from four testis samples collected at ZT1, ZT7, ZT13, and ZT19. All cells were clustered into six main cell types, including Sertoli cells, Leydig cells, macrophages, spermatogonia, spermatocytes, and spermatids. (**C**) Histogram of the normalized cell ratio in six cell clusters at four ZTs. (**D**) Heatmap of the top five differentially expressed genes (DEGs) in all six clusters. The representative markers are underlined in red. (**E**) Combined violin plot of the cell cluster markers expressed differentially in six cell clusters at four ZTs. (**F**) The bioluminescence recordings of the testes from *Tg(per3:luc)* after 10 days of light/dark cycle (LD) (cyan) or constant light (LL) (red) conditions ($n = 3$). (**G**) The amplitude statistics of bioluminescence in (F) ($n = 3$). (**H**) The fertilization rate of wild-type (WT) pairs with the males after 10 days of LD or LL conditions ($n = 7$). (**I**) The confocal images of the testes from *Tg(piwil1:mCherry)* after 10 days of LD or LL condition ($n = 4$). Scale bars, 100 μm. (**J**) The statistics of the germ cells in (I) ($n = 4$). $^*P < 0.05$, $^{**}P < 0.01$, and $^{***}P < 0.001$.

(Sertoli cells, Leydig cells, and macrophages) and germ cells (spermatogonia, spermatocytes, and spermatids) (Fig. 1B). Regarding the number of captured cells, the ratios of these six clusters differ across the four ZTs (Fig. 1C and fig. S1). The most significant variations were observed in spermatogonia, with the highest ratio at ZT13, and in spermatids, peaking at ZT19 (Fig. 1C), indicating that early spermatogenesis begins at ZT13 and spermatids mature at ZT19. The spermatogonial acrophase at ZT13 may result from rhythmic retinoic acid (RA) production in the testis, which drives nocturnal differentiation (*6*). The apoptosis could be another possibility of germ cell variation because rhythmic follicle-stimulating hormone or androgen can induce germ cell DNA damage/apoptosis (*24*). Macrophages are virtually undetectable at ZT13 (Fig. 1C). In contrast, most macrophages emerge at ZT19 and gradually decline in number until ZT7 (Fig. 1C), indicating daily fluctuations in immune cell numbers in the testis. Nonetheless, the proportions of these cell types were calculated from relatively small single-cell suspensions captured across four ZTs. Whether such daily variation of cellular numbers occurs in the testis requires further examination.

We then reanalyzed the six clusters based on a combination of scRNA-seq data from the four ZTs and identified marker genes, including previously unreported ones (Fig. 1D and table S1). In addition to the well-studied markers such as *ddx4* (*DEAD box polypeptide 4*; also known as *vasa*) (ENSDARG00000014373) (spermatogonia), *dmc1* (*DNA meiotic recombinase 1*) (ENSDARG00000055883) and *sycp3* (*synaptonemal complex protein 3*) (ENSDARG00000013438) (spermatocytes), *gsdf* (*gonadal somatic cell–derived factor*) (ENSDARG00000075301) (Sertoli cells), *star* (*steroidogenic acute regulatory protein*) (ENSDARG00000006137) and *cyp17a1* (*cytochrome P450, family 17, subfamily A, polypeptide 1*) (ENSDARG00000033566) (Leydig cells), and *apoa1a* (*apolipoprotein A-Ia*) (ENSDARG00000012076) and *apoa1b* (*apolipoprotein A-Ib)* (ENSDARG00000101324) (macrophages), previously unidentified markers are noteworthy, such as *tuba8l4* (*tubulin, alpha 8 like 4*) (ENSDARG00000006260) and *npm1a* (*nucleophosmin 1a*) (ENSDARG00000014329) (spermatogonia), *icn* (*ictacalcin*) (ENSDARG00000009978) (Sertoli cells), *tfa* (*transferrin-a*) (ENSDARG00000016771) (macrophages), and *fdx1b* (*ferredoxin 1b)*(ENSDARG00000038956) (steroidogenic cells of Leydig cells). Some well-known cellular markers, such as *gsdf*, *ddx4/vasa*, and *cyp17a1*, exhibit daily rhythmicity during the four ZTs (Fig. 1E), mirroring the temporal order of testicular physiology over a 24-hour period. We observed very low expression of *dmc1* and *cimap1b* (*ciliary microtubule–associated protein 1B*)/*odf3b* (*outer dense fibers of sperm tail 3b*) (ENSDARG00000114397) in somatic cells, which could result from contamination with attached sperm from some somatic cell suspensions.

To investigate whether external light affects spermatogenesis, we analyzed the testes of adult male zebrafish raised under constant light (LL) conditions. After 10 days of LL treatment, the amplitude of testicular bioluminescence rhythms of *Tg(per3:luc)* zebrafish was significantly reduced (Fig. 1, F and G), indicating disruption of the testis clock by LL. Moreover, this 10-day LL treatment also significantly reduced fertilization (Fig. 1H) and germ cells, as indicated by reduced fluorescent signals in the testes of *Tg(piwil1:mCherry)* zebrafish (Fig. 1, I and J), suggesting functional impairment. Overall, the testicular transcriptome revealed by the time-series scRNA-seq analysis indicates that spermatogenesis and somatic cells in the testis undergo rhythmic changes, possibly preparing for a rhythmic commitment to full gametogenesis.

Multiple testicular cells display daily rhythmicity

We have recently demonstrated that Sertoli cells display robust circadian rhythmicity (*6*). However, whether other testicular cell types exhibit daily rhythmicity remains unknown. Hence, we analyzed the rhythmicity of all testicular cell types (Fig. 2A), excluding macrophages, as none were detected at ZT13 (Fig. 1C). The circadian clock genes *arntl1a/bmal1a*, *cry2*, *csnk1db*, and *nfil3-2b* display daily rhythmicity in Sertoli cells (Fig. 2A). Spermatogonia also display rhythmic expression of key circadian clock genes (Fig. 2A). However, rhythmic expression of most key circadian clock genes, except *arntl1a/bmal1a*, is lost in spermatocytes, likely due to meiotic cycles interfering with the autonomous circadian clock (*3*, *9*, *25*), but is partially recovered in spermatids (Fig. 2A). We did not observe rhythmic expression of circadian clock genes in the Leydig cluster (Fig. 2A), likely because the number of captured Leydig cells was low (fig. S1). The expression patterns of key circadian clock genes vary in all testicular clusters (Fig. 2, A and B). We compared the expression patterns of key circadian clock genes in zebrafish testes, as revealed by time-series scRNA-seq, with those determined by time-series bulk RNA-seq (Fig. 2B and fig. S2A) (*6*). Key circadian clock genes, particularly *csnk1db* and *nfil3-2b*, exhibit significant rhythmic patterns with similar acrophases, as determined by time-series scRNA-seq (Fig. 2B) and by time-series bulk RNA-seq (fig. S2). We also compared the phases of key circadian clock genes across testicular cell types (Fig. 2C). Notably, *arntl1a/bmal1a* in Sertoli cells peaks during the day, whereas in spermatocytes, it peaks at night (Fig. 2C). This antiphasic expression may result in its arrhythmicity in the whole testis (fig. S2A). In contrast, the acrophages of *csnk1db* and *nfil3-2b* are less varied among testicular cell types (Fig. 2C), which could be a reason why these two genes display robust rhythmicity in the whole testis (fig. S2A).

In addition to circadian clock genes, we observed many rhythmically expressed genes in these five testicular clusters, including multiple marker genes and key functional genes in somatic and germ cells (Fig. 2D). In Leydig cells, marker *insl3* (*insulin-like* 3) (ENSDARG00000035862) and steroid-synthesizing enzymes encoding genes *cyp11a1* (*cytochrome P450 family 11 subfamily A member 1, tandem duplicate 1*) (ENSDARG00000002347) and *cyp17a1* are all rhythmically expressed in a daily cycle, although no circadian clock genes oscillate (Fig. 2, A and D). In Sertoli cells, *gsdf*, *cdh1* (*cadherin 1*) (ENSDARG00000102750), and *cdk1* (*cyclin-dependent kinase 1*) (ENSDARG00000087554) oscillate in a diurnal manner (Fig. 2D). In germ cells, *ccng1*(*cyclin G1*) (ENSDARG00000076667), *dazl* (*deleted in azoospermia-like*) (NSDARG00000036214), and *raraa* (*retinoic acid receptor, alpha a*) (ENSDARG00000056783) oscillate in spermatogonia; *ccnb3* (*cyclin B3*) (ENSDARG00000034855), *rec8b* (*REC8 meiotic recombination protein b*) (ENSDARG00000069260), and *ccbe1* (*collagen and calcium binding EGF domains 1*) (ENSDARG00000086158) oscillate in spermatocytes; and *izumo1*, *ift22* (*intraflagellar transport 22 homolog*) (ENSDARG00000020822), and *ift80* (*intraflagellar transport 80 homolog*) (ENSDARG00000038879) oscillate in spermatids (Fig. 2D). In general, Sertoli cells, spermatogonia, and spermatids display robust daily rhythmicity of key circadian clock genes, whereas Leydig cells and spermatocytes also exhibit rhythmic expression of functional genes, underscoring extensive daily rhythmicity across multiple somatic and germ cells of the zebrafish testis.

To investigate whether these rhythmically expressed genes are regulated by the circadian clock, we conducted quantitative reverse transcription polymerase chain reaction (qRT-PCR) to examine the

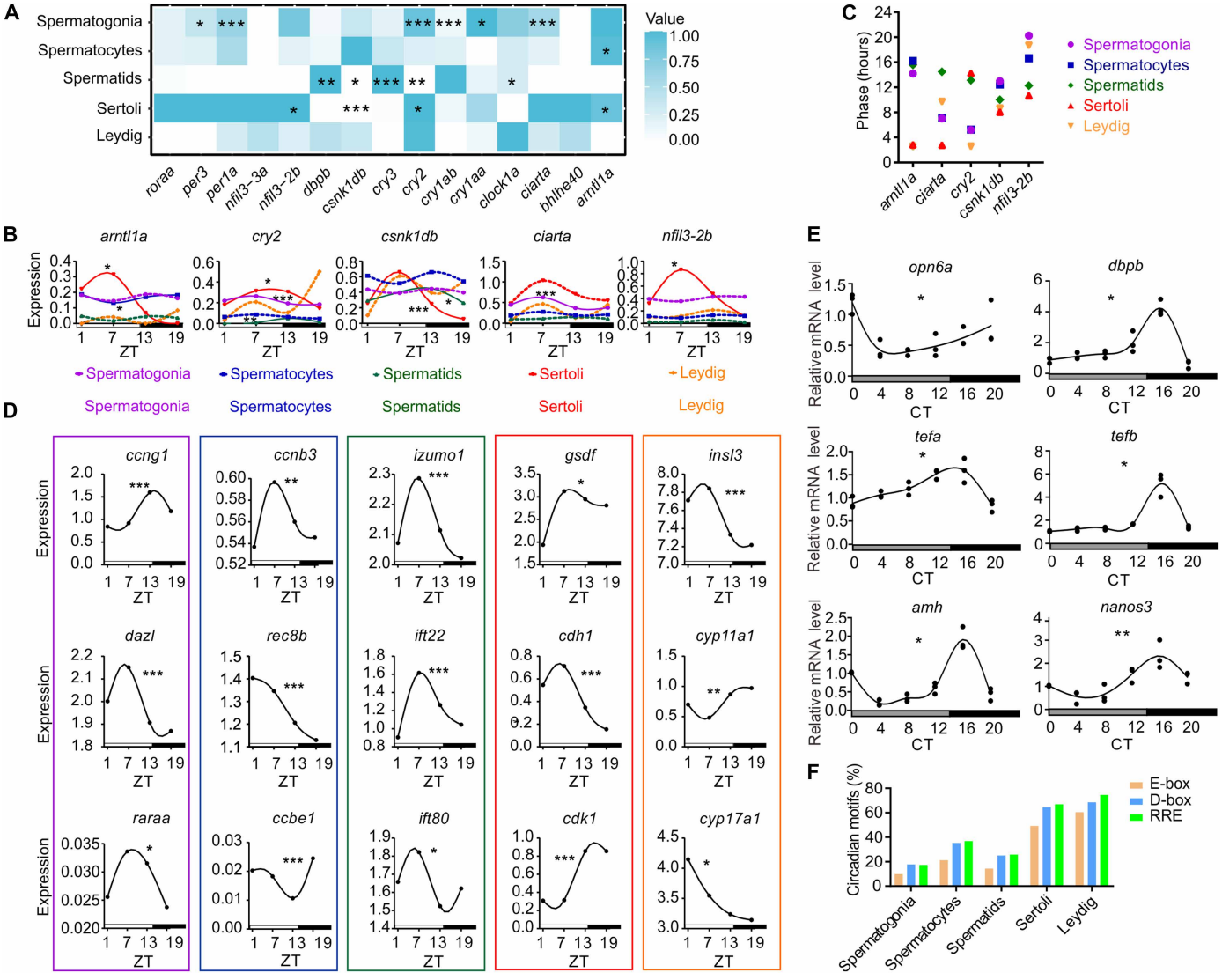

Fig. 2. Rhythmic expression of circadian clock genes and functional genes in five testicular cell types. (**A**) Heatmap of the average expression of core circadian clock genes in five clusters of the testis. The max-to-min value is normalized to 1 to 0. Values indicate normalized expression levels of circadian clock genes. A significant level indicates rhythmicity of key circadian clock genes. *P* values were calculated using MetaCycle ($n = 4$). (**B**) Rhythmic expression profiles of key circadian clock genes in five clusters of the testis, revealed by time-series scRNA-seq. The genes with significant rhythmicity are drawn in solid lines, and arrhythmic ones are drawn in dotted lines. (**C**) The acrophases of key circadian clock genes in five testicular cell types, as revealed by time-series scRNA-seq of the testis. The cell types are color coded, as shown in the legend. (**D**) The rhythmic expression of functional and marker genes in five types of testicular cells. $^{*}P < 0.05$, $^{**}P < 0.01$, and $^{***}P < 0.001$. (**E**) The relative mRNA level of key functional genes in the testis under constant darkness (DD) conditions, as shown by quantitative reverse transcription polymerase chain reaction (qRT-PCR). CT, circadian time. $n = 3 \times 3$. $^{*}P < 0.05$ and $^{**}P < 0.01$. (**F**) The percentages of key circadian motifs, Enhancer Box (E-box), Clock Regulatory Element D-box (D-box), and ROR Responsive Element/Retinoid Acid-Related Orphan Receptor Responsive Element (RRE/RORE), found in the promoters of the rhythmically expressed genes in five types of testicular cells.

expression of some of them, including opsin genes, circadian clock genes, and cell-specific markers in the testis under constant darkness (DD) conditions (Fig. 2E and fig. S2C). *opn6a* (*opsin 6*, *group member a*) (ENSDARG00000102430), *dbpb*, *tefa*, *tefb*, *amh*, and *nanos3* are all rhythmically expressed under DD conditions (Fig. 2E), indicating that they are regulated by the circadian clock. However, the qRT-PCR analyses using the bulk testicular RNA fail to detect the rhythmicity of the rhythmically expressed spermatogonial marker *raraa*, spermatocyte marker *ccnb3*, and Leydig cell marker *insl3* revealed by the time-series scRNA analysis under DD conditions (Fig. 2D and fig. S2C), which may result from that these genes have antiphasic expression patterns, such as *arntl1a/bmal1a*, in other testicular cell types, or that they are arrhythmic in most of the other testicular cell types. Then, we interrogated the 5′ 5000–base pair (bp) promoter sequences of all rhythmically expressed genes in these five testicular cell types and observed that most of them have at least one Clock Regulatory Element D-box (D-box), one Enhancer Box (E-box), or one ROR Responsive Element (RRE) motif in their promoter regions (table S2 and fig. S2D), implicating that they are likely regulated by the circadian clock. Rhythmically expressed genes in somatic cells,

including Sertoli cells and Leydig cells, appear to harbor more circadian motifs than those of germ cells, including spermatogonia, spermatocytes, and spermatids (Fig. 2F), suggesting stronger circadian regulation in somatic cells than in germ cells. We also wondered whether light is involved in regulating these rhythmically expressed genes. We observed that opsin genes *opn1mw4* (*opsin 1*, *medium-wave–sensitive*, *4*) (ENSDARG00000000638), *opn1sw2* (*opsin 1*, *short-wave–sensitive 2*) (ENSDARG00000017274), and *opn6a* are expressed primarily in germ cells rather than somatic cells (fig. S2B), suggesting that light may contribute more to the gene expression in germ cells. Together, most rhythmically expressed testicular genes, particularly those in somatic cells, revealed by scRNA analysis, are likely regulated by the circadian clock, whereas those rhythmically expressed genes in germ cells appear to be affected more by light.

Daily rhythmicity in cell-cell communications among testicular cells

In vertebrate testes, germ cells survive and develop in close and continuous interactions with somatic cells, such as Sertoli cells (*26*, *27*). The endocrine and supportive factors, such as RA from Sertoli cells and steroid hormones from Leydig cells, have been well characterized (*2*). In addition, numerous ligand-receptor–based cell-cell communications occur at cell junctions and adhesions (fig. S3). To investigate how cell-cell communications occur in the testis, we used both DanioTalk (*28*) and CellChat (*29*) to examine daily changes in ligand-receptor interactions (Fig. 3, A to C). Among the differentially expressed genes in cell clusters, most top-ranked cell-cell communications occur between Sertoli cells and other cell types (Fig. 3, A and B). Largely due to Sertoli cells' pivotal role in the testis (*6*, *30*, *31*), these dominant cell-cell interactions offer an opportunity to study Sertoli-cell–based communications. During the whole day, the number of cell-cell communications peaks at ZT1 and reaches the nadir at ZT7, with very few interactions between Sertoli cells and spermatocytes (Fig. 3 A, C, and D), while cell-cell communication strength peaks at ZT19 and reaches the nadir at ZT7 (Fig. 3, A and E). In general, cell-cell communications display daily rhythmicity, with the lowest levels in both quantity and strength at ZT7 (Fig. 3, D and E). Because this daily rhythmicity in cell-cell communications is primarily mediated by Sertoli cells, we further analyzed the ligand-receptor pairs originating from Sertoli cells (Fig. 3F). In the top pairs, Sertoli cells exhibit daily changes in their interactions with all germ cells except spermatids (Fig. 3F). The *angptl4* (angiopoietin-like 4) (ENSDARG00000035859)–*sdc2* (*syndecan 2*) (ENSDARG00000002731) and *angptl4*–*sdc4* (*syndecan 4*) (ENSDARG00000059906) pairs exhibit strong diurnal patterns, parallel to the daytime expression of *angptl4* in Sertoli cells (Fig. 3F). Sertoli cell–based cell-cell communications occur mostly with spermatogonia (Fig. 3, A, B, and F), probably reflecting the strong Sertoli cell–spermatogonia communications during spermatogonial differentiation. There are also daily changes in cell-cell interactions between Sertoli cells and Leydig cells (Fig. 3, A, B, and F). High cell-cell communications within the Sertoli cell cluster are also observed (Fig. 3, A, B, and F), indicating that Sertoli cell cooperation undergoes daily changes within the cyst envelope. Sertoli cells interact with a few macrophages at ZT1 and ZT19 (Fig. 3A), maybe as a complement to their immune function. We conducted time-series double-color fluorescence in situ hybridization (FIS on the testes under DD conditions using the ligand-receptor pair *angptl4* and *sdc4* (Fig. 3G). The adjacent expression patterns of *angptl4*, a Sertoli cell marker, and *sdc4*, expressed primarily in spermatogonia, spermatocytes, and spermatids, exhibit a preference for subjective daytime (Fig. 3G), corroborating their highest communication probability in ZT7 (Fig. 3F). In addition, to analyze daily Leydig cell–germ cell communications and avoid masking of Sertoli cells, we detected these cell-cell interactions only between Leydig cells and germ cells in the transcriptome (fig. S4, A and B). Those ligand-receptors display the most cell-cell communications at ZT1 and the lowest at ZT13 in Leydig cell–germ cell communications (fig. S4A), consistent with the highest expression of steroid-synthesizing enzymes encoding genes *cyp11a1* and *cyp17a1* in the night-to-day transition (Fig. 2C). We also identified ligand-receptor pairs originating from Leydig cells (fig. S4C). In the top pairs, Leydig cells interact rhythmically with spermatogonia (fig. S4C). However, the communication pairs between Leydig cells and spermatogonia, such as *angptl4*-*sdc4* and *cldn11a* (*claudin 11a*) (ENSDARG00000020031)–*cldn11b* (*claudin 11b*) (ENSDARG00000030723), display lower daily rhythmicity than those between Sertoli and spermatogonia (Fig. 3F and fig. S4C). Last, to investigate whether daily rhythmicity affects cellular synchrony among cysts, we examined testes from *clock1a*$^{-/-}$ and wild-type (WT) zebrafish using a scanning electron microscope (SEM) (Fig. 3H). The cyst compartments were not affected in *clock1a*$^{-/-}$ mutant zebrafish, indicating that the circadian clock synchronizes the cell fate and communication within the inner cyst rather than the inter cyst (Fig. 3H). Overall, cell-cell communications among testicular cells show daily rhythmicity in frequency and strength, supporting the pervasive daily rhythmicity of the zebrafish testis.

Daily rhythmicity of Sertoli cells and their previously unknown immune function

In vertebrate testes, spermatogenesis relies on the continuous development of both germ cells and somatic cells, which form cellular niches (*2*, *27*, *32*). In somatic cells, we first focus on Sertoli cells due to their pivotal role in the testis (*6*, *30*). In addition to the well-established Sertoli cell markers, we identified a previously unidentified marker, *icn*, as evidenced by its more extensive expression in Sertoli cells compared with *gsdf* (Figs. 1D and 4, A and C). The Sertoli cells with the cytoplasm and the nucleus stained by an *icn* probe are located outside of the cysts, which are full of germ cells stained by Hoechst (Fig. 4A). We reanalyzed the data and partitioned Sertoli cells into three subgroups defined by specific markers (Fig. 4B and table S3). As expected, two of the three subtypes (subtypes 0 and 2) contribute to the RA-producing function of Sertoli cells, as shown by colocalization of *aldh1a2*, encoding the rate-limiting enzyme in RA production (Fig. 4, B to D), with *gsdf* (Fig. 4C). The third subtype (subtype 1) exhibits the distinct expression pattern of immune cell marker *coro1a* (*coronin*, *actin-binding protein*, *1A*) (ENSDARG00000054610) (Fig. 4, B to D), which is known to be expressed in both blood cells and the immune system (*33*). Functionally, Sertoli cell subtype 0 contributes primarily to the homeostatic process and cytoplasmic translation with respect to the ribosomes (Fig. 4E), and the Sertoli cell subtype 2 focuses more on the cell cycle and reproductive process (Fig. 4G). In contrast, Sertoli cell subtype 1 is linked explicitly to immune processes, primarily regulating immune responses and promoting leukocyte migration (Fig. 4F and fig. S5A). Hence, it represents a potentially previously unknown role of Sertoli cells. We then crossed *Tg(coro1a:EGFP)* (*33*) with *Tg(gsdf:mCherry)* (*34*), generated double transgenic zebrafish *Tg(coro1a:EGFP;gsdf:mCherry)*, and examined how the previously undescribed immune subtype fits in the traditional Sertoli cells, as shown by *gsdf*$^{+}$ cells. The subtype of *coro1a*-marked Sertoli cells is

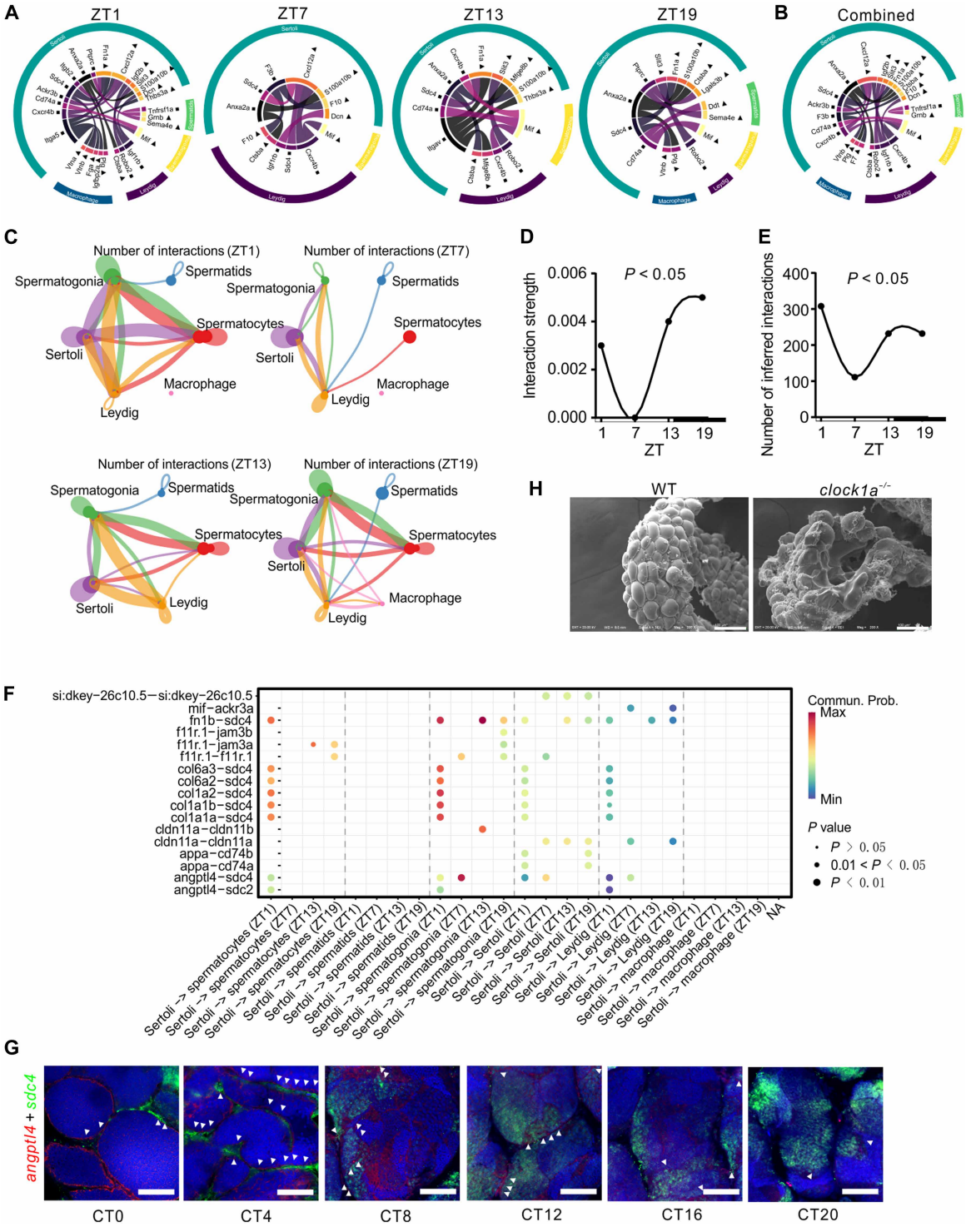

Fig. 3. Daily rhythmicity in cell-cell communications among testicular cell types. (**A** and **B**) Circle plot showing top-ranked ligand-receptor interactions in DEGs between testicular cells at four ZTs (A) and combined (B). Interactions were ranked on the basis of the differential expression of genes across clusters. The top 50-ranked interactions with the highest confidence cutoff (>900) are plotted. Triangles represent ligands, and rectangles represent receptors. *P*_value_cutoff = 0.05; FC_MIN_cutoff = 1.5. (**C**) Number of all ligand-receptor interactions between cell clusters at four ZTs. (**D** and **E**) Daily rhythmicity in the number of interactions (D) and their strength (E) at four ZTs. (**F**) The daily change of cell communication probability and significance between Sertoli cells and other cells in the testis, shown by top ligand-receptor pairs. NA, not applicable; Commun. Prob., communication probability. (**G**) Representative FISH images of ligand-receptor pair *angptl4-sdc4* in the testis under DD conditions, *angptl4* (red), a Sertoli cell marker, and *sdc4* (green), expressed primarily in spermatogonia, spermatocytes, and spermatids. The triangles indicate the area where the ligand-receptor pair is adjacently expressed in testicular cells. Scale bars, 50 μm. (**H**) Representative SEM images of testicular cysts in the testes of WT and *clock1a*$^{-/-}$ males ($n = 3$). Scale bars, 100 μm.

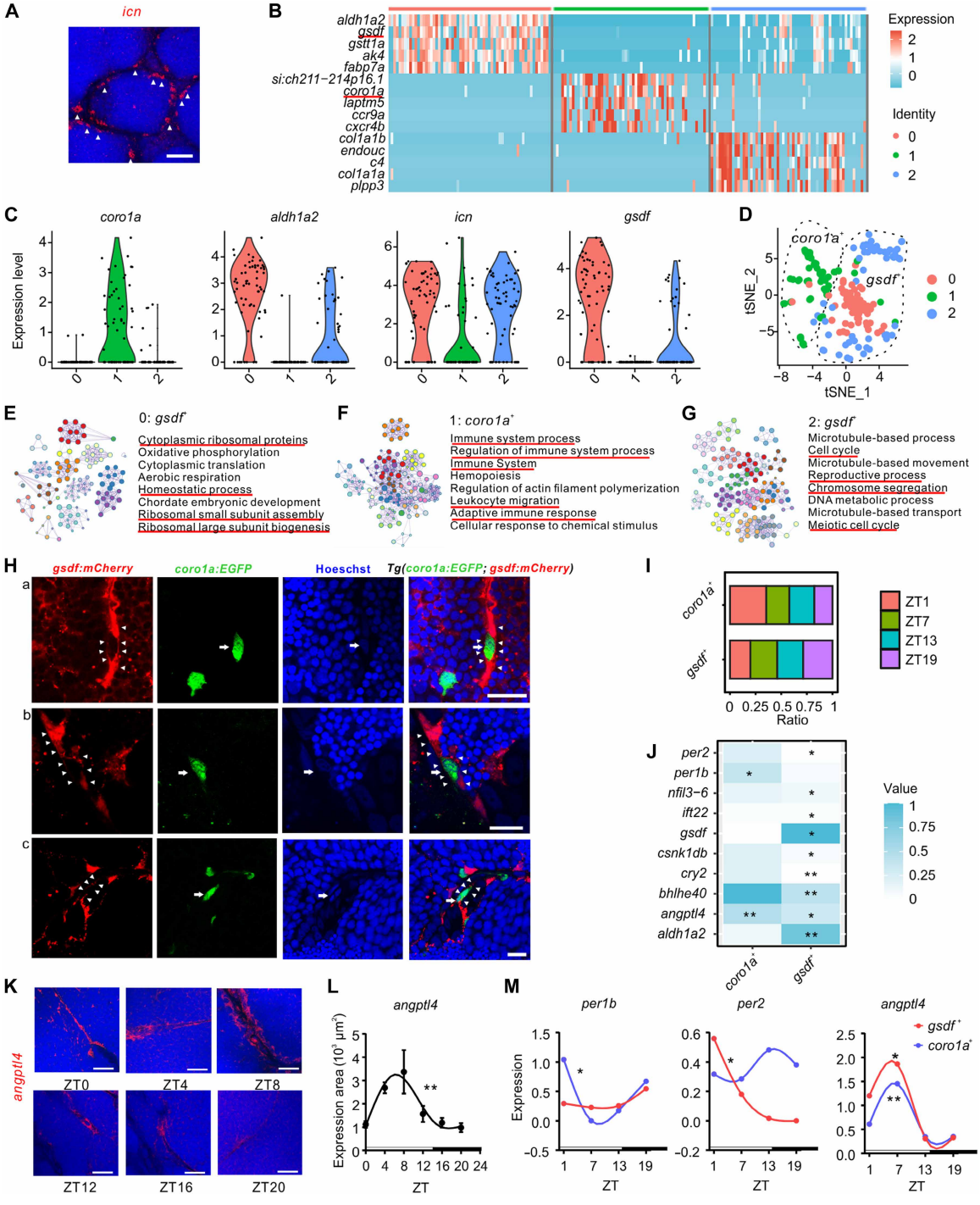

Fig. 4. Daily rhythmicity of Sertoli cells and characterization of the previously unidentified *coro1a*$^+$ Sertoli cell subtype. (**A**) A representative FISH image of the testis with *icn*. Arrowheads indicate Sertoli cells. All the nuclei are stained blue with Hoechst ($n = 3$). Scale bar, 15 μm. (**B**) Heatmap of the top five DEGs in the three Sertoli subtypes. Those markers under examination are underlined in red. (**C**) Violin plot of Sertoli cell markers expressed differentially in three subtypes. (**D**) tSNE dimensional reduction of Sertoli cells divided into three subgroups by distinct markers. Subgroups 0 and 2 are *gsdf*$^+$, while subgroup 1 is *coro1a*$^+$. (**E** to **G**) Metascape illustrations of top-enriched Gene Ontology (GO) annotations in the three subtypes 0 (E), 1(F), and 2 (G) of Sertoli cells. (**H**) Representative FISH images of Sertoli cells in the testis of double transgenic zebrafish *Tg(coro1a:EGFP;gsdf:mCherry)*. Three representative views are shown in panels (a) to (c). All the nuclei are stained blue with Hoechst. Arrowheads indicate *gsdf*$^+$ Sertoli cells, and arrows indicate *coro1a*$^+$ Sertoli cells. Scale bars, 15 μm. $n = 3$. (**I**) Histogram of the normalized cell ratio in the *gsdf*$^+$ subtype and the *coro1a*$^+$ subtype at four ZTs. (**J**) Rhythmic expression of key circadian clock genes and other genes in the two subtypes. $n = 4$. *$P < 0.05$ and **$P < 0.01$. (**K** and **L**) Representative FISH images of testicular cells with *angptl4* in the testis (K) and their quantification and statistical analysis (L). All the nuclei are stained with Hoechst. Scale bars, 15 μm. *P* values were calculated using MetaCycle. $n = 6 \times 2$. **$P < 0.01$. (**M**) Rhythmic expression profiles of key circadian clock genes and other genes in the two subtypes over the four ZTs. Significant rhythmicity marked with asterisks; *$P < 0.05$ and **$P < 0.01$.

embedded or adjacent to the traditional subtype of *gsdf*$^+$ Sertoli cells (Fig. 4H), as shown in double transgenic zebrafish *Tg(coro1a:EGFP; gsdf:mCherry)* (Fig. 4H). Both subtypes composed an integrated constitution of the testicular envelope of the cyst (Fig. 4H). Hence, we designated subtypes 0 and 2 of Sertoli cells as *gsdf*$^+$ and subtype 1 as *coro1a*$^+$, respectively (Fig. 4D).

Regarding cell numbers, both Sertoli cell subtypes exhibit daily rhythmicity, with *gsdf*$^+$ cells most active at ZT19 and *coro1a*$^+$ cells most active at ZT1 (Fig. 4I), indicating circadian regulation of Sertoli cells, consistent with our recent study (*6*). We also examined the expression of circadian clock genes across all three Sertoli cell subtypes (Fig. 4J and fig. S5B). Several circadian clock genes, including *per2* and *cry2*, as well as their rhythmic markers *gsdf* and *aldh1a2*, are all rhythmically expressed in *gsdf*$^+$ cells (Fig. 4J). In contrast, only *per1b* is rhythmically expressed in *coro1a*$^+$ cells (subtype 1). Hence, the daily rhythmicity is more robust in *gsdf*$^+$ Sertoli cells (Fig. 4J and fig. S5B). In addition to key circadian clock genes, *angptl4* is also rhythmically expressed in Sertoli cells (Fig. 4, J to M, and fig. S5B), as shown by both scRNA-seq (Fig. 4, J and M, and fig. S5B) and time-series FISH on the testes (Fig. 4, K and L). Together, Sertoli cells are responsible not only for RA production and for supporting spermatogenesis but also for immune regulation and for protecting the germinal compartment.

Previously unidentified subtypes of Leydig cells and macrophages

We then characterize the remaining two somatic cell types, i.e., Leydig cells and macrophages. The Leydig cells play a fundamental role in male gonad development by dictating steroid production (*2*, *21*, *27*). All Leydig cells express genes encoding key enzymes in male hormone production, including *star*, *cyp17a1*, *cyp11c1*, and *hsd11b2* (*hydroxysteroid 11-beta dehydrogenase 2*) (ENSDARG00000001975) (Fig. 1D and table S3). *fdx1b*, encoding the mitochondrial redox partner required for cortisol production (*35*), is expressed in Leydig cells, as shown by both the scRNA analysis (Fig. 1D) and double-color FISH (Fig. 5A). Genes involved in *jun/fos* signaling are highly expressed in one subtype of Leydig cells (Fig. 5, B and C) and are enriched for key cellular processes, such as cell cycle, apoptosis, and immune responses (fig. S6C). Hence, we designated this Leydig cell subtype as *jun/fos*$^+$, consistent with previous studies on the role of Activator Protein 1 (AP-1) signaling in Leydig cells (*36*–*39*), and the other subtype as *rps27.2*$^+$ (*Ribosomal protein S27*, *isoform 2*; ENSDARG00000055475), which is its top marker gene. Steroidogenic regulatory factors such as *star*, *cyp17a1*, *cyp11c1*, and *insl3* are expressed in both Leydig cell subtypes (fig. S6B).

Testicular macrophages promote testicular homeostasis (*40*) and are identified by multiple markers, including *apoa1a*, *apoa1b*, *apoa2* (*apolipoprotein A- II*) (ENSDARG00000015866), and *apoeb* (*apolipoprotein Eb*) (ENSDARG00000040295) (Fig. 1, D and E, and table S3). In addition, a previously unidentified marker, *tfa*, is highly expressed in macrophages, as shown in the region between the cysts, as shown by the scRNA analysis (Fig. 1D) and double-color FISH (Fig. 5E). Gene Ontology (GO) annotations reveal its roles in the immune system, response to estrogenic stimulus, biological oxidations, and multiple catabolic processes (fig. S6D). Within macrophages, two subtypes can be distinguished by differential expression of marker genes (Fig. 5, F and G). We then named the two subtypes after their top-expressed genes, *fgb*$^+$ (*fibrinogen beta chain*) (ENSDARG00000008969) and *hmgn2*$^+$ (*high mobility group nucleosomal binding domain 2*) (ENSDARG00000099572) (Fig. 5, F to H), respectively. We performed time-series FISH on the testes under DD conditions using a *tfa* probe and observed that macrophage numbers peak at night (Fig. 5, I and J), consistent with our time-series scRNA-seq analysis (Fig. 1C). The significant circadian fluctuations in macrophage numbers indicate that the testicular microenvironment undergoes pronounced changes over 24 hours (Figs. 1, C to E, and 5, I and J), underscoring the need to collect samples at multiple time points over consecutive 24 hours to better elucidate the testicular immune system.

Spermatogonia differentiate nocturnally

Following a continuous differentiation trajectory, 28,798 germ cells collected over 24 consecutive hours allow us to map distinct germ cell states from spermatogonia to spermatocytes and then to spermatids (Fig. 1B). To understand the initiation and development of spermatogenesis over a single day, we perform a Monocle pseudotime analysis (*41*, *42*) of spermatogonia and recluster them (Fig. 6, A and B). Spermatogonia differentiate from early stem cells to those that commit to meiosis (Fig. 6B). We analyzed differentially expressed genes along the pseudotime from type A to type B spermatogonia (Fig. 6C), as indicated by the transition from undifferentiated to differentiating spermatogonia (*43*). In the developmental order of gametogenesis, clustering analysis reveals four cohorts of dynamic events, comprising two up-regulated and two down-regulated cohorts (Fig. 6C). Down-regulated events include ribosome biogenesis, translation, posttranslational protein modification, and the immune system. In contrast, up-regulated events include cilium movement, cell cycle, meiotic cell cycle, and reproductive processes (Fig. 6C). The onset of spermatogenesis is defined by the expression of spermatogonial markers *nanos2*, *nanos3*, and *ddx4/vasa* (Fig. 1, D and E, and table S1), as previously reported (*6*, *34*, *44*, *45*). Then, we found that more genes are explicitly expressed in spermatogonia (Fig. 1D and table S1). In particular, previously undescribed markers, *npm1a* and *tuba8l4*, are expressed in spermatogonia (Fig. 6, D and E), as shown by FISH. Cell fate and proliferation in development follow a long, continuous trajectory, describing a smooth progression to a differentiated state with distinct states separated by several directions (Fig. 6, A and F). The presence of distinct states and continuous transitions is substantiated over 1 day (Fig. 6G), during which early markers such as *nanos2*, *nanos3*, *npm1a*, and *zbtb16a* are down-regulated while *sycp1*, *tekt1* (*tektin 1*) (ENSDARG00000101331), and *zte38* (*zebrafish testis–expressed 38*) (ENSDARG00000037056) are up-regulated (fig. S7B). However, *tuba8l4* is first up-regulated and then down-regulated (fig. S7, A and B). The Monocle pseudotime analysis reveals significant daily rhythmicity of spermatogonia with a nocturnal pattern (Fig. 6H). In the temporal order of differentiation, maturation of spermatogonia peaks at ZT19, indicated by the biggest pseudotime value over 1 day, consistent with the acrophase of *aldh1a2* and RA production in Sertoli cells at night (Fig. 4J). Time-series FISH on the testes under DD conditions using a *ddx4* probe showed that spermatogonia develop in a circadian manner, peaking at night (Fig. 6, J and K), in line with the pseudotime analysis (Fig. 6H). Because there are two branches in the differentiation of spermatogonia (Fig. 6, A, B, F, and G), we used Branch Expression Analysis Modeling (BEAM) analysis (*41*, *42*) to assess cellular significance at both branches (Fig. 6, L and M). In branch one, six annotations show opposite trends in states 2 and 5. Genes involved in autophagy, apoptotic process, programmed cell death, cilium organization, microtubule-based transport, meiotic

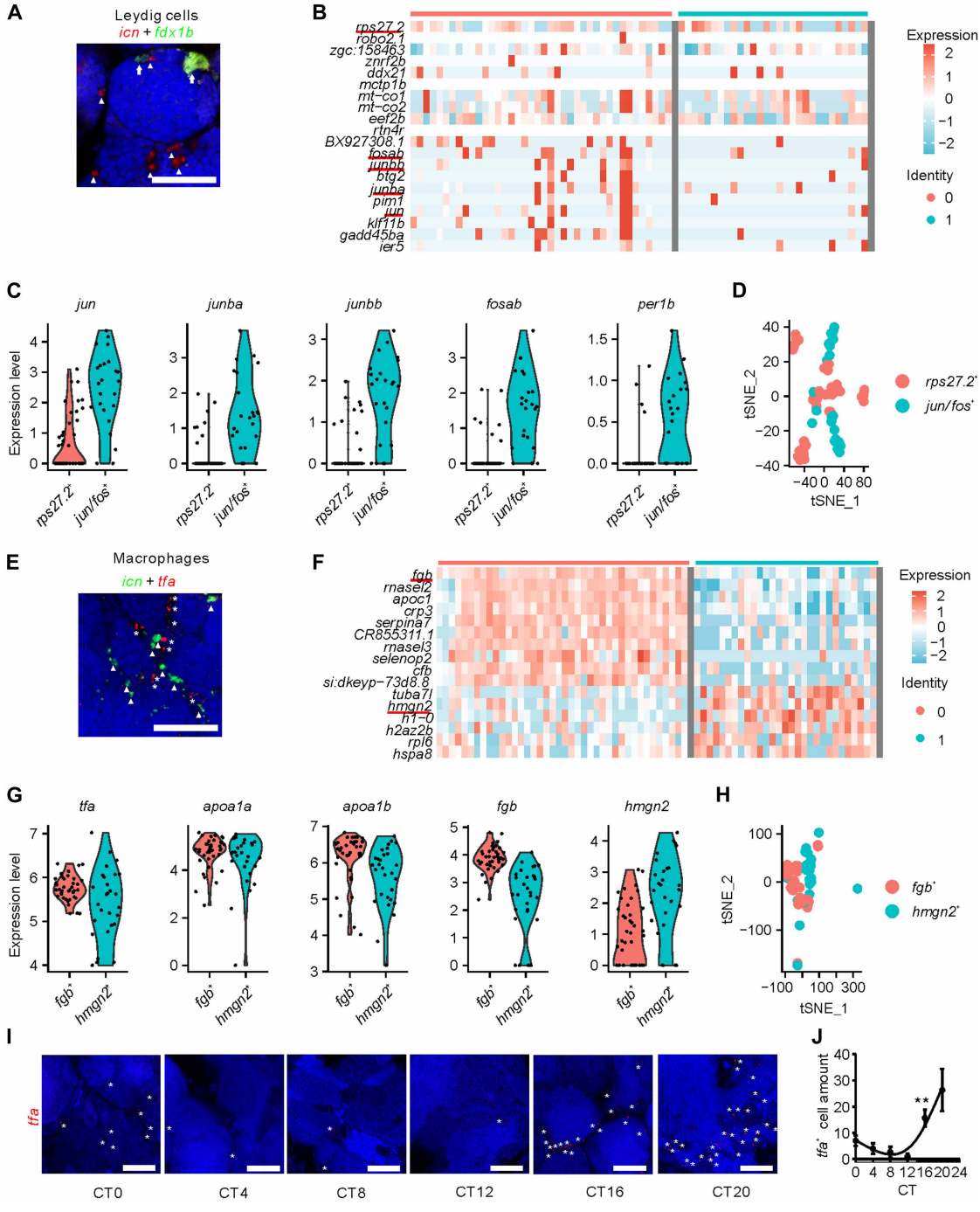

Fig. 5. Characterization of the subtypes of Leydig cells and macrophages. (**A**) A representative FISH image of the testis with the Leydig cell marker *fdx1b* probe (green) and the Sertoli cell marker *icn* probe (red). All the nuclei are stained blue with Hoechst. Scale bar, 50 μm. Arrows indicate Leydig cells, and arrowheads indicate Sertoli cells. $n = 3$. (**B**) Heatmap of the top 10 cell markers in the two Leydig cell subtypes. Those markers related to *rps27.2* and *jun/fos* signaling are underlined in red. (**C**) Violin plot of the expression of markers of *jun/fos* signaling and circadian clock gene *per1b* in Leydig cell subtypes. (**D**) tSNE plot of the two Leydig cell subtypes. (**E**) A representative FISH image of the testis with macrophage marker *tfa* probe (red) and the Sertoli cell marker *icn* probe (green). Asterisks indicate macrophages, and arrowheads indicate Sertoli cells. All the nuclei are stained blue with Hoechst. Scale bar, 50 μm. $n = 3$. (**F**) Heatmap of the top DEGs in the two macrophage subtypes. Those markers used to name the subtype clusters are underlined in red. (**G**) Violin plot of the representative markers of the two macrophage subtypes. (**H**) tSNE plot of the two macrophage subtypes. (**I** and **J**) Representative FISH images of testicular cells with the *tfa* under DD conditions (I) and their quantification and statistical analysis (J). All the nuclei are stained with Hoechst. Asterisks indicate macrophages. Scale bars, 50 μm. *P* values were calculated using MetaCycle. $n = 6 \times 3$. $^{**}P < 0.01$.

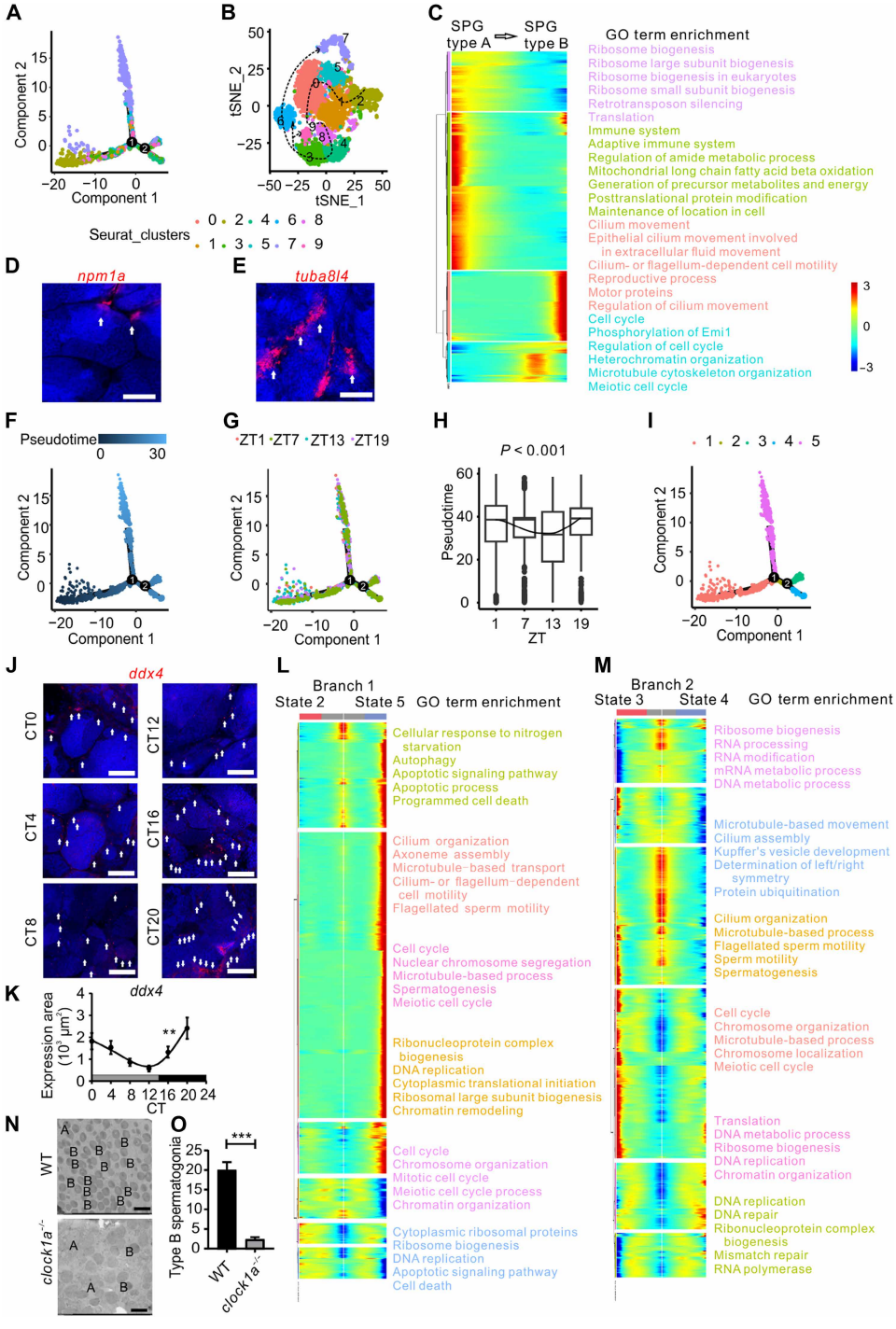

Fig. 6. Spermatogonia differentiation peaks at ZT19. (**A**) Pseudotime trajectory of the spermatogonia with Monocle analysis. Cells are colored according to the clusters in spermatogonia. (**B**) tSNE dimensional reduction of spermatogonia divided into 10 subgroups by Seurat. The dashed line indicates the differentiating direction according to pseudotime analysis in (A). (**C**) Heatmap of 1000 DEGs by Monocle pseudotime in the direction of spermatogonia differentiation. SPG, spermatogonia. (**D** and **E**) Representative FISH images of the testis with *npm1a* (D) and *tuba8l4* (E). All the nuclei are stained blue with Hoechst. Scale bars, 50 μm. Arrows indicate spermatogonia ($n = 3$). (**F** and **G**) Pseudotime trajectory of the spermatogonia with Monocle analysis. Cells are colored according to pseudotime (F) or original ZTs (G). (**H**) Pseudotime values of spermatogonia across four ZTs. (**I**) Pseudotime trajectory of the spermatogonia with Monocle analysis. Cells are colored according to whether they are prebranch or postbranch. (**J** and **K**) Representative FISH images of testicular cells with *ddx4* under DD conditions (J) and their quantification and statistical analysis (K). All the nuclei are stained with Hoechst. Arrows indicate spermatogonia. Scale bars, 50 μm. *P* values were calculated using MetaCycle. $n = 6 \times 3$. $^{**}P < 0.01$. (**L** and **M**) Heatmap of BEAM clustering of DEGs ($n = 3000$) in two branches, 1 (L) and 2 (M), in spermatogonia. Each row represents a gene, and each column represents a single cell, with columns/cells placed in pseudotime order defined in (I). (**N**) Representative transmission electron microscopy (TEM) images of testicular sections from *clock1a*$^{-/-}$ and WT male zebrafish ($n = 3$). Spermatogonia type A and spermatogonia type B are indicated as A and B. Scale bars, 5 μm. (**O**) The statistics of the type B spermatogonia cells in (M) ($n = 3$). $^{***}P < 0.001$.

cell cycle, and spermatogenesis are up-regulated in state 5 but down-regulated in state 2 (Fig. 6L), indicating increased meiosis and cell fate transitions in state 5. The other three clusters exhibit the down-regulation of genes involved in DNA replication, cytoplasmic translational initiation, microtubule-based processes, chromatin remodeling, chromosome organization, ribosome biogenesis, and cell death in state 5 (Fig. 6L). In branch two of spermatogonia, opposite trends in states 3 and 4, including ribosome biogenesis, microtubule-based movement, cilium organization, cell cycle, translation, and DNA repair, indicate a complex regulation in the cell fate of spermatogonia during differentiation (Fig. 6M).

To investigate whether the internal clock affects the cell fate in the nocturnal differentiation of spermatogonia, we examined spermatogonia types in the testes of the *clock1a*$^{-/-}$ mutant (*6*) and WT zebrafish. While numerous type B spermatogonia are developed in the WT testis, the *clock1a*$^{-/-}$ mutant testis has only a few type B spermatogonia (Fig. 6, N and O), suggesting that loss of Circadian locomotor output cycles kaput 1a (Clock1a) impairs spermatogonia differentiation. Together, spermatogonia differentiation displays daily rhythmicity, peaking at night, and the circadian clock is required for differentiation from type A to type B spermatogonia.

Spermatocytes undergo maturation nocturnally

We also performed pseudotime analysis of meiotic cells (Fig. 7A). The unbiased development of spermatocytes indicates only fate, provided that those germ cells undergo meiosis (Fig. 7, A and B). Spermatocytes develop over 1 day (Fig. 7C), and maturation levels peak at ZT13 (Fig. 7D). We performed time-series FISH on the testis under DD conditions using a *dmc1* probe and observed that spermatocytes mature in a circadian pattern, peaking at night (Fig. 7, G and H), consistent with the pseudotime analysis (Fig. 7D). To understand the cellular transitions from primary to secondary spermatocytes, we analyzed the differentially expressed genes in spermatocytes along the pseudotime (Fig. 7E). In the developmental order of spermatocytes, clustering analysis reveals four groups of dynamic events, comprising two up-regulated and two down-regulated groups (Fig. 7E). Down-regulated events include ribosome biogenesis, translation, chromatin organization, and protein folding, while up-regulated events consist of microtubule-based processes, cilium organization, cell cycle, spermatogenesis, and chromosome segregation (Fig. 7E). In this process, spermatogonial markers, such as *ddx4* and *piwil*, are down-regulated, whereas meiotic markers, such as *cdk2*, *dmc1*, and *sycp3*, are initially up-regulated and subsequently down-regulated (fig. S9A). These known markers were further corroborated by previously unidentified markers: *ndel1a* (*nudE neurodevelopment protein 1-like 1*) (ENSDARG00000010953) and *hmgb1a* (*high mobility group box 1a*) (ENSDARG00000099175) (Fig. 1D and fig. S9A). These marker genes are differentially expressed among all spermatocytes, with *hmgb1a* being the most robustly expressed (Fig. 7F). Furthermore, *hmgb1a* is rhythmically expressed, peaking at ZT7 (Fig. 7I), which falls within the time when spermatocytes develop (Fig. 7, D, F, G, and H). To investigate whether the rhythmicity of *hmgb1a* is regulated by the circadian clock, we isolated an *hmgb1a* promoter harboring an ROR Responsive Element/Retinoid Acid-Related Orphan Receptor Responsive Element (RRE/RORE) motif and ligated it to the vector pGL4.17 (Fig. 7J). Luciferase reporter assays showed that *hmgb1a* is activated by the Roraα but repressed by Rev-erbα, and deleting the RRE/RORE motif abolishes the transactivation activities (Fig. 7J); subsequently, chromatin immunoprecipitation (ChIP) assays showed that Roraα binds to the RRE/RORE motif of *hmgb1a* (Fig. 7K), indicating that *hmgb1a* is regulated directly by the circadian clock via the RRE/RORE motif. To investigate whether *hmgb1a* functions in meiosis, we generated a heterozygous *hmgb1a*$^{+/-}$ mutant using CRISPR-Cas9 (Fig. 7L and fig. S8, A to F), as homozygous *hmgb1a*$^{-/-}$ zebrafish appear to be embryonic lethal. The spermatocytes marked by *sycp3* are significantly reduced even in heterozygous *hmgb1a*$^{+/-}$ mutant testes, as shown by FISH (Fig. 7, L and M), supported by significant down-regulation of *sycp3* in the *hmgb1a*$^{+/-}$ mutant testes, as determined by qRT-PCR (Fig. 7N). Together, these results show that spermatocytes exhibit a nocturnal preference and that the circadian clock–regulated *hmgb1a* plays a critical role in meiosis.

Nocturnal preference in cell fates of spermatids

To investigate how the final state of germ cells develops following pseudotime ordering from spermiogenesis, we calculated pseudotime trajectories of postmeiotic cells (Fig. 8A). At the final stage of gametogenesis, spermatids exhibit two unexpected directions of development (Fig. 8, A and B). Cell fates exhibit distinct time-of-day–specific preferences in the three states of spermiogenesis (Fig. 8, C to G). In all spermatids, maturation shows a significant nocturnal pattern (Fig. 8D). Early spermatids develop, peaking at ZT19 (Fig. 8E), when two branches emerge with distinct time preferences: state 2, with its peak at ZT7, and state 3, with its peak at ZT1 (Fig. 8, F and G). To determine the cell-fate states of the two states, we used BEAM analysis (*41*, *42*) to detect differences in the two branches after state 1 (Fig. 8H). In the clustering analysis, six annotations show opposite trends in states 2 and 3. Protein autophosphorylation, oxidative phosphorylation, cytoplasmic translation, and metabolism of RNA are increased in state 2 but decreased in state 3 (Fig. 8H), indicating reduced protein translation and posttranslational modification in state 3. The other four clusters exhibit increased activity in cell cycle, microtubule-based processes, chromosome segregation, DNA damage response, DNA repair, protein deubiquitination, cilium assembly, and cilium organization in state 3 (Fig. 8H). In addition, markers of meiosis are increased, whereas those of spermiogenesis are decreased in state 3 (Fig. 8I). To further explore how spermatids differ between states 2 and 3, we examined the testis using FISH with a *cimap1b*/*odf3b* probe, a marker of spermatids (Fig. 8J). *cimap1b*/*odf3b* is expressed at a higher level in the early stage of spermatid E1 rather than the very-late spermatid E2 or spermatid E3 (Fig. 8J). *cimap1b*/*odf3b* is expressed at a higher level at stage 2 than at stage 3 in spermatids (Fig. 8I), suggesting that stage 3 represents a very late stage of spermatid development, likely corresponding to mature spermatids. Those genes related to cilia and circadian clocks also differ between states 2 and 3 (fig. S9), suggesting that cilia and circadian clocks may be involved in the cell-fate decision during the final stage of gametogenesis. Together, the final stage of spermiogenesis exhibits a complex pattern of cell fates, with a nocturnal developmental preference.

DISCUSSION

In this study, we performed a time-series scRNA-seq analysis of 29,315 cells from the zebrafish adult testis over 24 consecutive hours to examine the daily rhythmicity of somatic and germ cells. Integrating rhythmicity analysis, pseudotime trajectory inference, and intercellular communication modeling, we uncover pervasive daily programs across germ cells, somatic cell types, and intercellular communication networks; identify previously unreported immune-competent Sertoli

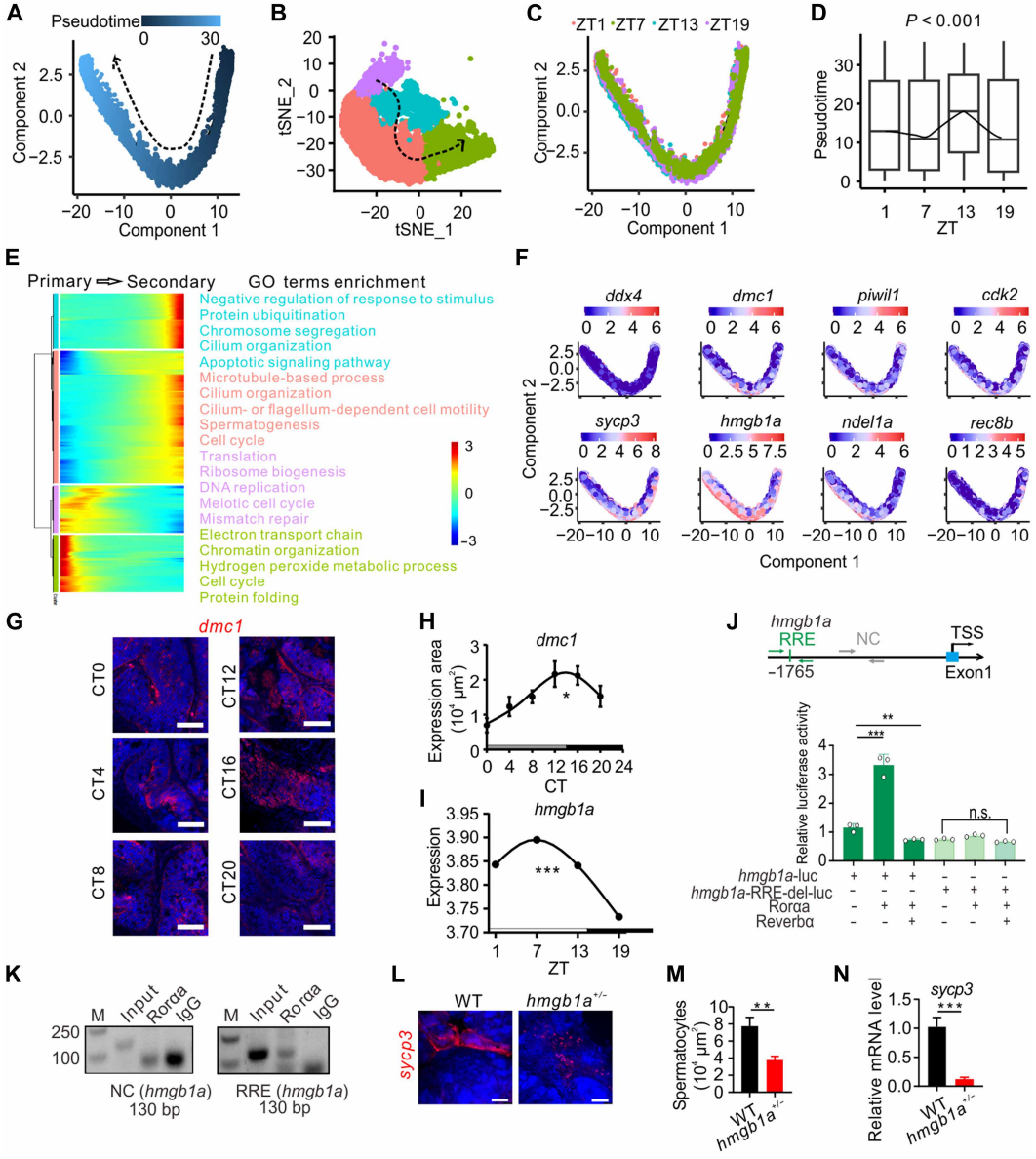

Fig. 7. Spermatocytes undergo meiosis nocturnally, and *hmgb1a* is required for spermatocyte development. (**A**) Pseudotime trajectory of the spermatocytes with Monocle analysis. Cells are colored by pseudotime. The dashed line indicates the direction of development according to pseudotime analysis. (**B**) tSNE dimensional reduction of spermatocytes divided into four subgroups by Seurat. The dashed line indicates the direction of differentiation according to pseudotime analysis in (A). (**C**) Pseudotime trajectory of spermatocytes with Monocle analysis. Cells are colored according to original ZTs. (**D**) Pseudotime values of spermatocytes across four ZTs. (**E**) Heatmap of 1000 DEGs by Monocle pseudotime in the direction of spermatocyte development. The top GO terms associated with germ cells during developmental transitions are divided into four clusters, each color coded for up-regulation or down-regulation. (**F**) Relative expression of key spermatocytes markers by pseudotime. Cells are colored according to pseudotime. (**G** and **H**) Representative FISH images of testicular cells with *dmc1* in the testis under DD conditions (G) and their quantification and statistical analysis (H). All the nuclei are stained with Hoechst. Scale bars, 50 μm. *P* values were calculated using the MetaCycle. $n = 6 \times 3$. $^{**}P < 0.01$. (**I**) Rhythmic expression of the spermatocyte marker *hmgb1a* over four ZTs. $^{***}P < 0.001$. (**J**) Diagram of the *hmgb1a* promoter harboring an RRE/RORE motif and luciferase reporter assays. $n = 3$. $^{**}P < 0.01$ and $^{***}P < 0.001$. n.s., not significant. (**K**) ChIP assays. (**L** and **M**) Representative FISH images of the testis from *hmgb1a*$^{+/-}$ and WT male zebrafish with *sycp3* (L) and their quantification and statistical analysis (M). All the nuclei are stained blue with Hoechst. Scale bars, 50 μm. $n = 4$. $^{**}P < 0.01$. (**N**) Relative mRNA level of *sycp3* in the *hmgb1a*$^{+/-}$ and WT testes. $n = 3$. $^{***}P < 0.001$.

subtypes; and demonstrate that spermatogenesis follows a nocturnal developmental schedule. In particular, Sertoli cells, spermatogonia, and spermatids exhibit robust rhythmic expression of key circadian clock genes (Fig. 2A). Cell-cell communications show daily variations in quantity and strength (Fig. 3), which may fine-tune temporal synchronization in the testis. We also identified previously undescribed subtypes of Sertoli cells (Fig. 4), Leydig cells (Fig. 5), and macrophages (Fig. 5). Pseudotime trajectory analysis over 24 hours, used in circadian biology, demonstrates that the spermatogenic process exhibits a nocturnal preference in all functional phases (fig. S10). As a whole, the testis is a temporally coordinated organ with pervasive daily rhythmicity.

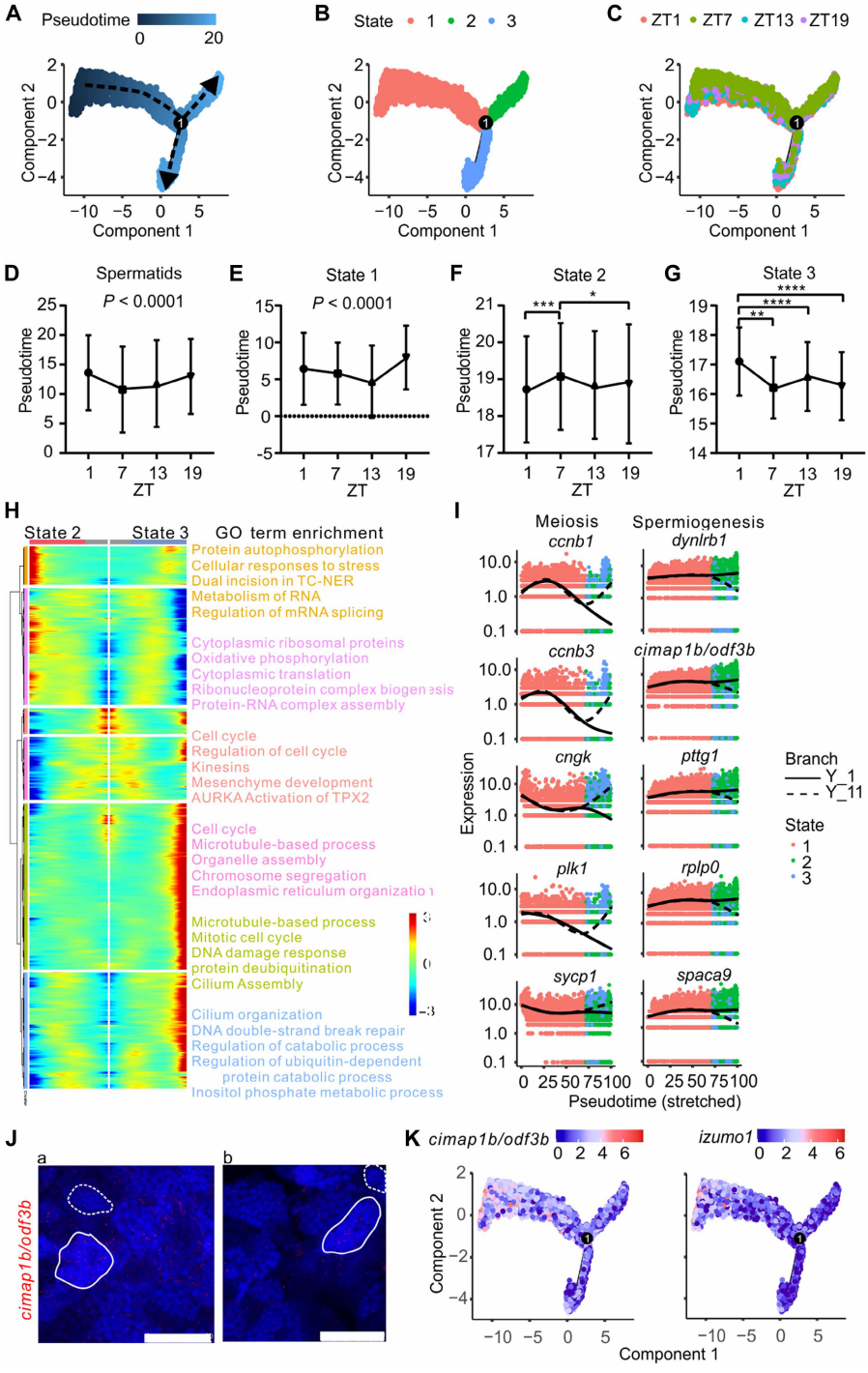

Fig. 8. Nocturnal preference in cell fates of spermatids. (**A**) Pseudotime trajectory of spermatids with Monocle analysis. Cells are colored according to the pseudotime. The dashed line indicates the direction of development according to pseudotime analysis. (**B** and **C**) Pseudotime trajectory of the spermatids with Monocle analysis. Cells are colored according to the cell state (B) and original ZTs (C). (**D**) Pseudotime values of spermatids over four ZTs. (**E** to **G**) Pseudotime values for States 1 (E), 2 (F), and 3 (G) in spermatids over four ZTs. *P* value is determined by one-way analysis of variance (ANOVA). $*P < 0.05$, $**P < 0.01$, $***P < 0.001$, and $****P < 0.0001$. (**H**) Heatmap of BEAM clustering of DEGs ($n = 3000$) in two branches after early state 1 in spermatids. Each row represents a gene, and each column represents a single cell, with columns/cells placed in pseudotime order defined in (A). DEGs are clustered into six groups, and the top five GO annotations enriched using Metascape v3.5 are given on the right of the corresponding gene clusters. (**I**) Expression of key spermatid DEGs by pseudotime. Two branches indicate dynamic patterns of representative genes. The trends of dynamics after the branch in the left panel (meiosis genes) are opposite those in the right panel (spermiogenesis genes). (**J**) Representative FISH images of the testis with the spermatid marker *cimap1b/odf3b* probe (red). Two representative views are shown in panels (a) and (b). All the nuclei are stained blue with Hoechst. Spermatids circled with solid lines indicate early spermatids, E1 or E2. Spermatids circled with dashed lines indicate mature spermatids, E3. Scale bars, 50 μm. $n = 3$. (**K**) The expression patterns of germ cell markers *cimap1b/odf3b* and *izumo1* in spermatids are depicted by pseudotime.

Daily rhythmicity of Sertoli cells, spermatogonia, spermatids, and cell-cell communications in the testis

Daily rhythms in the testis transcriptome have been observed in zebrafish, mouse, and baboon (*6*, *22*). Although ~5% of genes in the zebrafish testis exhibit rhythmic expression, only a few key clock genes are rhythmic (*6*). In particular, Sertoli cells display distinct clock activity and function as the driver of the testis clock (*6*). However, it is unclear whether other testicular cells exhibit daily rhythmicity. In this study, we used time-series scRNA-seq analysis over 24 hours to investigate daily rhythmicity in all testicular cells, except macrophages, which were not detected at ZT13 (Fig. 1C). In somatic cells, Sertoli cells show significant daily rhythmicity of several key circadian clock genes (Fig. 2A), consistent with our previous observation (*6*). In addition to circadian clock genes, we show that *angptl4* is rhythmically expressed in Sertoli cells (Fig. 4, J to M, and fig. S5B). Future studies should examine its rhythmic function in Sertoli cells. Although no rhythmicity in circadian clock gene expression was observed in Leydig cells, we found rhythmic expression of *cyp11a1* and *cyp17a1*, which encode steroidogenic enzymes, in Leydig cells (Fig. 2C), indicating rhythmic steroidogenesis in the testis, as previously reported (*4*, *5*, *9*). In germ cells, both spermatogonia and spermatids display daily rhythmicity in several key circadian clock genes, whereas spermatocytes exhibit rhythmic expression of only *arntl1a/bmal1a* (Fig. 2A), suggesting that profound meiotic epigenetic and metabolic reprogramming may interfere with circadian clock function. This is consistent with dampened clock gene expression in mouse spermatocytes (*3*), suggesting evolutionary conservation of clock suppression during meiotic prophase. We also observed that *arntl1a/bmal1a* is expressed in spermatocytes and Sertoli cells in an antiphasic manner (Fig. 2C), indicating a complex circadian regulation in the testis. Nevertheless, oscillations in *ccnb3*, *rec8b*, and *ccbe1* persist in spermatocytes (Fig. 2C). It will be interesting to investigate whether rhythmic *arntl1a/bmal1a* regulates these functional genes in spermatocytes in the future. However, the spermatids partially recover clock rhythmicity during the final stage of spermatogenesis (Fig. 2A). Our time-series qRT-PCR and FISH results show that numerous rhythmically expressed genes revealed by our scRNA analysis maintain their rhythmicity under DD conditions (Figs. 2E, 5, I and J, 6, J and K, and 7, G and H), indicating that circadian regulation dictates them. Furthermore, bioinformatic interrogation of 5′ upstream promoter sequences of all rhythmically expressed testicular genes revealed that most of them harbor at least one circadian motif, such as E-box, D-box, or RRE motif (Fig. 2F, fig. S2D, and table S2), pointing to their potential circadian regulation. Together, the complex circadian rhythmicity in testicular cells highlights the importance of timed orchestration and communication throughout the testis.

Testicular cells engage in complex communication networks to coordinate the various functions within the testis (*46*–*49*). Testicular paracrine signaling has been well studied, i.e., Leydig cells produce testosterone, and Sertoli cells secrete RA and activin, which act on neighboring cells to regulate their functions, respectively (*26*, *27*, *50*). In addition, cellular communications have been studied in a juxtacrine manner through direct cell-cell interactions mediated by cell-surface receptors and ligands, which are crucial for supporting and differentiating germ cells during spermatogenesis (*51*–*53*). These diverse communications within the testis allow for the integration of various signals, the coordination of cellular functions, and the maintenance of the delicate balance required for proper testicular development and function (*27*, *50*, *53*). However, it remains unclear whether these testicular cell-cell communications exhibit daily rhythms (Fig. 3, A to H). We observed robust daily rhythmicity in cell-cell communications within testicular cells, especially between Sertoli cells and other cell types (Fig. 3, A to H). Sertoli cells can interact with and regulate the functions of various testicular cell types, including macrophages, Leydig cells, and spermatogenic cells, within the testicular microenvironment (Fig. 3, A to H). Furthermore, the strength of cell-cell communications exhibits a nocturnal pattern, peaking at ZT19 (Fig. 3, D and E). In the top communication pairs, very few were observed between Sertoli cells and spermatids, indicating that these interactions occur infrequently during late gametogenesis (Fig. 3F). In addition, interactions between Sertoli cells and macrophages help maintain the delicate balance between immune surveillance and immune tolerance in the testis (Fig. 3A) (*26*, *50*, *54*). The ligand-receptor pairs *angptl4-sdc2* and *angptl4-sdc4* have been reported in the key processes of human germline development and cancer progression (*55*, *56*). Our time-series double-color FISH indicates rhythmic cell communication between *angptl4* and *sdc4* during zebrafish germ cell development (Fig. 3, F and G). However, future studies are needed to validate these rhythmic cell-cell communications functionally.

Although our testicular samples in the scRNA analysis were collected under light/dark cycle (LD) conditions, making it difficult to discern the circadian rhythmicity of these testicular cells, numerous rhythmically expressed genes indeed maintain their rhythmicity in the testis under DD conditions, as shown by qRT-PCR or FISH, and the promoters of most of the rhythmically expressed testicular genes have circadian regulatory motifs, as determined by bioinformatic interrogation, all pointing to their circadian regulation. However, future investigation should use time-series scRNA analysis of testicular samples under DD conditions over 48 hours to ascertain the circadian rhythmicity of these testicular cells. While our study captured rarer somatic populations, future studies using somatic cell enrichment strategies will provide even deeper insights into their full rhythmic potential.

Previously unknown characteristics of somatic cells and their rhythmic immunity

Although identifying previously unrecognized somatic cell populations is important for studying gonadal function, new somatic cell subtypes have rarely been identified in previous scRNA-seq studies of the testis (*20*, *57*–*59*). Here, we used 517 somatic cells from four time points over a consecutive 24-hour period to uncover rare or previously unrecognized cell populations. We identified a previously unrecognized immune cell population in Sertoli cells, characterized by high expression of *coro1a* (Fig. 4, B to F). While Sertoli cells are known to phagocytose apoptotic germ cells (*60*), our data suggest that this *coro1a*$^{+}$ Sertoli cell subtype is closely aligned with or embedded in *gsdf*$^{+}$ cells within the cyst envelope (Fig. 4H). Whether these cells directly interact with macrophages or modulate the blood-testis barrier rhythmically remains to be examined in the future.

In Leydig cells, we identified a *jun/fos*$^{+}$ subtype marked by the AP-1 family (Fig. 5, B to D). Members of the AP-1 family play critical roles in regulating Leydig cell function, including steroidogenesis, differentiation, proliferation, and response to hormonal and environmental stimuli (*61*–*63*). We named the other Leydig cell subtype as *rps27.2*$^{+}$. Notably, steroidogenic regulatory factors such as *star*, *cyp17a1*, *cyp11c1* (*cytochrome P450*, *family 11*, *subfamily C*, *polypeptide 1*) (ENSDARG00000042014), and *cyp11a1* are also expressed in this Leydig cell subtype (fig. S6B). Macrophages, which were not identified in a

previous zebrafish study (*21*), are predominantly present at ZT19 but are rarely detected at other times of day, as shown by our scRNA analysis (Fig. 1C), corroborated by our time-series FISH analysis of the testes under DD conditions (Fig. 5, I and J). We classified macrophages into two subtypes, *fgb*$^{+}$ and *hmgn2*$^{+}$ (Fig. 5, F to H), which should set the stage for future investigation of their functions in testicular macrophages. Notably, the emergence of macrophages at night could indicate nocturnal adaptation and migration. It appears that macrophages exhibit increased migration and tissue-specific distribution at night, migrating more actively to specific sites of potential infection or injury (*64*). These nighttime-specific changes in macrophage activity may be responsible for clearing apoptotic cells generated during peak spermatogenesis and have been regarded as an evolutionary adaptation, allowing the immune system to be more vigilant and responsive to potential threats at night, when the body is more vulnerable to infections and other challenges (*64*).

Spermatogenesis is organized synchronously in a nighttime preference

Our merged scRNA-seq datasets also reveal the rhythmic patterns in testicular germ cell differentiation and development. This is the first time pseudotime analysis has been applied to investigate cellular development in a rhythmic manner, although the method has been widely used in single-cell studies of development (*17*–*20*). In the onset of spermatogenesis, spermatogonia undergo a rest-active phase transition to subsequent mitotic divisions (Fig. 6, F to H). The highest maturation of spermatogonia occurs at night, as evidenced by pseudotime analysis (Fig. 6H) and time-series FISH with *ddx4* (Fig. 6, J and K). The nocturnal maturation of spermatogonia coincides with rhythmic RA production in Sertoli cells and rhythmic expression of RA receptors in spermatogonia (Figs. 2C and 4, H and J). Spermatocytes undergoing meiosis show the highest level of maturation, with a coordinated phase at ZT13 by pseudotime analysis (Fig. 7D) and peaking at ZT12 by time-series FISH with *dmc1* (Fig. 7, G and H). We found that *hmgb1a* is rhythmically expressed in spermatocytes (Fig. 7I) and is regulated by the circadian clock via an RRE/RORE motif (Fig. 7, J and K). *hmgb1a* belongs to the HMG family of proteins with various functions (*65*) and was recently found to respond to bacterial infection in zebrafish neutrophils (*66*). We observed that rhythmically expressed *hmgb1a* contributes to spermatocyte development, as evidenced by a significant reduction of spermatocytes (Fig. 7, L and M) and down-regulation of *sycp3* (Fig. 7N) in *hmgb1a*$^{+/-}$ mutant testes. However, the mechanism underlying Hmgb1a's role in spermatocytes remains to be investigated in the future.

The spermatids undergo spermiogenesis, a process that entails flagellum development and nuclear condensation, ultimately giving rise to mature sperm (*2*, *15*, *67*). This differentiation process is accompanied by programmed cell death (apoptosis), which also occurs in other phases of spermatogenesis, to ensure the quality of the final sperm, or through phagocytosis by Sertoli cells, which degrade spermatids that fail to complete maturation (*2*, *68*, *69*). In zebrafish (Fig. 7A), as in humans but unlike mice, spermatids exhibit a pronounced bifurcation in the pseudotime trajectory, indicating two subgroups with distinct transcriptomes late in spermatid development (*1*). Specifically, one subgroup of spermatids maintains or increases the expression of key spermiogenesis genes, such as *cimap1b*/*odf3b*, *spaca9* (*sperm acrosome-associated 9*) (ENSDARG00000068130), and *pttg1* (*PTTG1 regulator of sister chromatid separation*, *securin*) (ENSDARG00000075421), whereas the other subgroup fails to increase expression and even decreases them (Fig. 8H). The synchronous maturation of spermatids during early daylight is likely the result of a series of timing signals during spermiogenesis, such as the rhythmic secretion of RA, to prepare for potential fertilization. We conducted FISH using *cimap1b*/*odf3b* to examine different stages of spermatids (Fig. 8J) and observed that the early stage of spermatid E1 has higher expression of *cimap1b*/*odf3b*, which then tapers off in the very-late spermatid E2 or spermatid E3 (Fig. 8J). In general, zebrafish testicular germ cells develop with a nocturnal preference (fig. S10). Hence, it is tempting to speculate that nocturnal spermatogenesis may reflect an evolutionary adaptation, i.e., because zebrafish spawn at dawn, completing spermatid maturation by early morning (ZT1 to ZT7) ensures optimal sperm availability, and synchronizing meiosis (ZT13) and spermiogenesis (ZT19) to the night phase minimizes oxidative damage from light exposure or align with systemic hormone rhythms (e.g., melatonin).

Although our time-series scRNA-seq under LD conditions cannot pinpoint the circadian rhythmicity of the zebrafish testis, we have shown that disruption of the testis clock by 10 days of LL treatment significantly reduces both spermatogenesis (Fig. 1, I and J) and fertilization (Fig. 1H). We also examined the effects of Clock1a on spermatogonia differentiation and testicular cyst compartments. Loss of Clock1a arrests spermatogonia differentiation from type A to type B (Fig. 6M) but does not affect the testicular cyst compartments (Fig. 3G). Hence, it appears that the circadian clock is essential for numerous testicular developmental, differentiational, and reproductive processes, which warrants their future validation under constant darkness.

In conclusion, our time-series single-cell atlas fundamentally revises the view of the testis from a largely arrhythmic organ to one orchestrated by pervasive daily rhythms. We demonstrate that daily rhythmicity extends beyond Sertoli cells to germ cells and is embedded in a concerted nocturnal preference of spermatogenesis. We identify previously undescribed somatic subtypes, such as the immune-competent *coro1a*$^{+}$ Sertoli cells, and reveal rhythmic intercellular communication networks as a previously unappreciated layer of temporal coordination. Our study establishes the zebrafish as a powerful model for unraveling how diurnal rhythms coordinate complex reproductive processes in vertebrates.

MATERIALS AND METHODS

Animals

Zebrafish (*Danio rerio*) WT AB strain and transgenic and mutant lines are maintained at 28.5°C on a 14-hour/10-hour light/dark cycle at the Soochow University Zebrafish Facility, in accordance with standard protocols (*70*). The Soochow University Animal Ethics and Use Committee approved all zebrafish protocols (no. SUDA20230811A01). Transgenic line *Tg(coro1a:EGFP;gsdf:mCherry)* was obtained by crossing *Tg(coro1a:EGFP)* (*33*) with *Tg(gsdf:mCherry)* (*34*). Transgenic lines *Tg(per3:luc)* (*16*) and *Tg(piwil1:mCherry)* (*6*) were raised under LD conditions and then transferred to LL conditions for 10 days to examine the male fertility.

Generation of *hmgb1a*$^{+/-}$ mutant zebrafish

The *hmgb1a*$^{+/-}$ mutant was generated with CRISPR-Cas9 as previously described (*6*). Briefly, the guide RNA (gRNA) site (AAGAACTACATTCCACCCAAAGG) was selected in Exon 2 of *hmgb1a*,

containing a Bsl1 enzyme site for genotyping (fig. S8A). Synthesized gRNA and Cas9 mRNA were first microinjected into one-cell embryos. Enzymatic digestion of PCR products from the targeted fragment was used to estimate gRNA efficiency, which was 66% (fig. S8B). The microinjected embryos were raised to adulthood. The adult mutant lines were screened by PCR using fin-clipped DNA, and the results were confirmed by sequencing. The *hmgb1a*$^{+/-}$ mutant zebrafish with a 4-bp deletion (fig. S8C), resulting in premature truncation (fig. S8D), were characterized at the F_1 generation, as the homozygous mutants appeared to be embryonic lethal. *hmgb1a* is reduced ~50% in *hmgb1a*$^{+/-}$ mutant zebrafish (fig. S8, E and F).

scRNA-seq and bulk RNA-seq analyses of the zebrafish testes

The testes were collected from two 3-month-old zebrafish males at each of the following time points: ZT1, ZT7, ZT13, and ZT19 over consecutive 24 hours. Before sample collection, we housed 3-month-old males in groups of 20 in a 10-liter tank for 1 month, without a mating schedule, to rule out potential effects of mating behavior at light onset. The zebrafish started locomotor activity as usual at ZT0 when the light was turned on. Subsequently, single-cell suspensions from each sample were prepared as previously described (*6*) and subsequently loaded into a Chromium microfluidic chip, which was barcoded using a 10× Chromium Controller (10x Genomics). RNAs from the barcoded cells were reverse transcribed, and sequencing libraries were constructed with reagents from a Chromium Single-Cell reagent kit (10x Genomics) according to the manufacturer's instructions. Sequencing was performed with Illumina NovaSeq 6000 according to the manufacturer's instructions (Illumina). Raw reads were demultiplexed and mapped to the reference genome (Zebrafish GRCz11) by 10x Genomics Cell Ranger pipeline using default parameters. A total of 29,315 cells was captured and analyzed from these four testis samples (approximately 7000 cells per sample). All subsequent single-cell analyses were performed using Cell Ranger and Seurat packages (*71*). Briefly, for each gene and each cell barcode (filtered by Cell Ranger), unique molecule identifiers were counted to construct digital expression matrices. Secondary filtration was performed by Seurat, i.e., a gene expressed in more than three cells was considered expressed, and each cell was required to have at least 50 expressed genes. Cells with higher mitochondrial RNA (mtRNA) expression were excluded. The raw and processed data have been deposited at the National Center for Biotechnology Information (NCBI) under accession GSE206024. In the scRNA-seq analysis of the zebrafish testis, feature-barcode matrices were generated, and the Seurat package was used for data normalization, dimensionality reduction, clustering, and differential expression analysis. For clustering, principal components analysis was performed on highly variable genes. The top principal components were used for graph-based clustering in Seurat with a resolution parameter of 1.0. The zebrafish testis cells are divided into six clusters, including spermatogonia, spermatocytes, spermatids (including spermatozoa), Sertoli cells, Leydig cells, and macrophages (Fig. 1C). We also conducted time-series bulk RNA-seq of zebrafish testes each with two duplicates collected for two consecutive days with a 4-hour interval under LD condition, each sample with mixed testes from 3- to 4-month-old adult fishes (*6*). RNA-seq–based transcriptome analysis was conducted as described previously (*72*). Total RNAs from each sample were extracted with TRIzol (Invitrogen). The RNA-seq of these testicular total RNAs was performed as follows. (i) library construction for sequencing, (ii) clustering and sequencing, (iii) quality control, and (iv) transcriptome assembly. These clean reads were mapped to the zebrafish genome (GRCz11). Only reads with a perfect match or one mismatch were further analyzed and annotated on the basis of the reference genome. The raw data were deposited at the NCBI with Sequence Read Archive (SRA) accession number PRJNA579855.

Fluorescence in situ hybridization

In situ hybridization assays using digoxigenin-labeled probes to detect the expression of *icn*, *tfa*, *npm1a*, *tuba8l4*, *ddx4*, *dmc1*, *sycp3*, *cimap1b/odf3b*, and *angptl4* were performed on the testicular sections or whole-mount testes as previously described (*6*). The DNA fragments used to synthesize RNA probes were amplified by PCR using testicular cDNAs and the primers listed in table S4. All RNA probes were in vitro transcribed using a digoxigenin labeling mixture (Roche, 11277073910). Dual FISH was performed on whole-mount testis as previously described (*6*). RNA probes of *fdx1b* and *sdc4* were labeled with a Fluorescein RNA Labeling Mixture (Roche, 11685619910). Briefly, the fixed tissue was permeabilized with protein K for 30 min. The antisense RNA probes were incubated with the samples at 65°C for 16 hours, and the colors were developed by Alexa Fluor 488 or Alexa Fluor 555 (Invitrogen, B40912 and B40923), respectively. Each in situ hybridization was performed at least three times, with at least three testes per hybridization ($n = 3 \times 3$).

Rhythmicity analyses

To identify rhythmically expressed genes in scRNA-seq data, we used the MetaCycle package, using pseudoreplicates as previously described (*73*). This approach was used to overcome the limitation of having only one biological replicate per time point at the cellular level, thereby enabling the application of MetaCycle's statistical framework. Briefly, we treated each cell within a cluster as a replicate and randomly assigned it to one of three pseudoreplicates at each ZT time point. The three matrices of mean values for each cluster were computed using MetaCycle to assess rhythmicity. In bulk RNA-seq data, the average Fragments Per Kilobase of transcript per Million mapped reads (FPKM) values from two replicates across the 12 time points were analyzed using MetaCycle to assess rhythmicity. Genes were considered to be rhythmically expressed when the integrated *P* value was <0.05. The two-day bulk RNA-seq data were averaged to compare with the 1-day scRNA-seq data (fig. S2).

DanioTalk and CellChat

DanioTalk is a computational method for inferring and analyzing intercellular communication networks from scRNA-seq data, specifically for zebrafish (*D. rerio*) studies (*28*). Both the initial ligand and membrane receptor lists for zebrafish were manually curated on the basis of gene descriptions and localization records for human orthologs in the COMPARTMENTS database and the Human Protein Atlas (*28*). We installed and loaded the DanioTalk package as an R package from GitHub. We identified ligand-receptor interactions between cell types using the runDanioTalk function on differentially expressed genes within clusters. In DanioTalk, the plotNetwork function enabled us to visualize the communication network, the strength of ligand-receptor interactions, and the activation of signaling pathways. To compare communication networks across multiple ZT time points, we used the compareCommunicationNetworks function to analyze intercellular communication networks and identify

changes in communication patterns associated with specific biological processes or developmental stages.

CellChat is also a tool for analyzing cell-cell communications from scRNA-seq data (*29*). We installed CellChat as an R package for Bioconductor. To run the CellChat analysis, we first loaded the scRNA-seq data and cell-type annotations and then identified ligand-receptor interactions between cell types. Then, we constructed the intercellular communication network and visualized the results. We also used the netVisualbubble function to identify the signaling roles of different cell types within the network and to compare their intercellular communication networks. Both DanioTalk and CellChat were used to cross-validate findings and ensure robustness.

Monocle pseudotime analysis

Trajectory analysis was performed using Monocle (*41*, *74*). To infer the pseudotime trajectory, we used the orderCells function to infer the pseudotime trajectory from the dimensionally reduced data. We specified a "root" cell or cell type to define the starting point of the trajectory. To analyze the pseudotime trajectory, we identified genes or pathways that were differentially expressed along it using the differentialGeneTest function. We used the plot_complex_cell_trajectory function to explore branching points in the trajectory. Subsequently, we assigned the pseudotime-dependent gene-expression patterns to the underlying biological processes involved in cell differentiation and development.

Imaging acquisition and analysis

The fluorescent images of the testes from green fluorescent protein (GFP)/mCherry-transgenic zebrafish or FISH assays were acquired using a confocal microscopy system (Leica SP8) with laser emissions at 405, 488, and 543 nm. All nuclei are counterstained with Hoechst 33342 to allow accurate staging based on nuclear morphology in the zebrafish testis. The intensities of positive cells in distinct colors were quantified using ImageJ (National Institutes of Health).

Bioluminescence analysis of the zebrafish testis

LumiCycle-based bioluminescence assays were conducted to examine testes from adult zebrafish *Tg(per3:luc)* as previously described (*6*). At least three testes were used for each transgenic zebrafish line, and each LumiCycle assay was performed at least three times ($n = 3 \times 3$). Waveforms of rhythmic bioluminescence emission were analyzed using the LumiCycle software package.

SEM and transmission electron microscopy

Zebrafish testicular samples were fixed in 2.5% glutaric dialdehyde (Sigma-Aldrich, G5882) buffer and embedded for 24 hours, and their SEM/transmission electron microscopy (TEM) images were acquired with SEMs (Hitachi, S-4700 Field Emission Scanning Electron Microscope or ZEISS EVO 18 Scanning Electron Microscope) at the Soochow University Electron Microscopy Core Facility.

Luciferase reporter assays

Luciferase reporter assays were performed as previously described (*75*). Briefly, the 2-kb 5′ *hmgb1a* promoter fragment was isolated by PCR and subcloned into the luciferase reporter vector pGL4.17. JASPAR (https://jaspar.genereg.net) analysis (*76*) showed that the *hmgb1a* promoter contains one RRE motif (5′-AGGTCA-3′). Deletion of this regulatory motif was done with the Mut Express II Fast Mutagenesis Kit (Vazyme, catalog no. C214). pcDNA3.1 plasmids of full-length cDNAs of Rorαa and Rev-erbα-His were reported previously (*77*). The cotransfection experiments were carried out with 293T cells with Lipofectamine 2000 (Invitrogen, catalog no. 11668027) according to the manufacturer's instructions. Luciferase reporter assays were performed with a Dual-Report assay system (Promega, catalog no. E1980). Three independent experiments were conducted.

ChIP assays

ChIP assays were conducted as previously described (*78*). Rorαa-His was synthesized by mMESSAGE mMACHINE T7 (Invitrogen, catalog no. 01149314) and then microinjected into one-cell zebrafish embryos. Embryos were collected at 24 hours postfertilization. DNA bound by Rorαa was immunoprecipitated using an anti–6 × His antibody (Abcam, catalog no. ab213204) and a ChIP assay kit (Merck, catalog no. 4000321). Last, the ChIP results were analyzed using PCR. The primers used are listed in table S4.

RNA extraction and qRT-PCR

Total RNAs were extracted from 3-month-old zebrafish testes collected under DD conditions with MicroElute Total RNA Kit (Omega, R6831). cDNAs were synthesized with oligo(dT) for mRNA. Then, qRT-PCR was performed on an ABI StepOnePlus instrument using the SYBR Green detection system (Takara) with a thermal profile of 40 cycles of 95°C for 10 s and 60°C for 30 s. Each qRT-PCR was performed with at least three different biological samples, each in triplicate ($n = 3 \times 3$). All results were normalized to the expression level of the housekeeping gene β-actin.

Bioinformatic interrogation of circadian motifs in the promoter sequences of rhythmically expressed testicular genes

The circadian clock regulates its downstream genes through cis-regulatory elements, including E-box, D-box, and RRE/RORE motifs (*79*–*81*). We searched for these circadian motifs in the noncoding regions of rhythmically expressed testicular genes, as previously described (*79*, *80*). Briefly, 5′ upstream 5000-bp promoter sequences of all rhythmically expressed testicular genes revealed by the scRNA analysis were downloaded from Ensembl BioMart in batch for zebrafish genes (GRCz11) and were analyzed with the Find Individual Motif Occurrences (FIMO) tool (*82*). FIMO scanned the promoter sequences to detect matches for E-box, D-box, or RRE/RORE motifs. The FIMO matches were filtered before output, with a match *P* value threshold set to 0.01.

Statistical analysis

Values are means ± SD of the indicated number of measurements. Statistical significance was determined using one-way analysis of variance (ANOVA) or Student's *t* test with a significance of $P < 0.05$.

Supplementary Materials

The PDF file includes:

Table S4
Figs. S1 to S10
Legends for tables S1 to S3

Other Supplementary Material for this manuscript includes the following:

Tables S1 to S3

REFERENCES

1. B. P. Hermann, K. Cheng, A. Singh, L. Roa-De La Cruz, K. N. Mutoji, I. C. Chen, H. Gildersleeve, J. D. Lehle, M. Mayo, B. Westernstroer, N. C. Law, M. J. Oatley, E. K. Velte,

B. A. Niedenberger, D. Fritze, S. Silber, C. B. Geyer, J. M. Oatley, J. R. McCarrey, The Mammalian spermatogenesis single-cell transcriptome, from spermatogonial stem cells to spermatids. *Cell Rep.* **25**, 1650–1667.e8 (2018).
2. R. W. Schulz, L. R. de Franca, J. J. Lareyre, F. Le Gac, H. Chiarini-Garcia, R. H. Nobrega, T. Miura, Spermatogenesis in fish. *Gen. Comp. Endocrinol.* **165**, 390–411 (2010).
3. J. D. Alvarez, D. Chen, E. Storer, A. Sehgal, Non-cyclic and developmental stage-specific expression of circadian clock proteins during murine spermatogenesis. *Biol. Reprod.* **69**, 81–91 (2003).
4. J. D. Alvarez, A. Hansen, T. Ord, P. Bebas, P. E. Chappell, J. M. Giebultowicz, C. Williams, S. Moss, A. Sehgal, The circadian clock protein BMAL1 is necessary for fertility and proper testosterone production in mice. *J. Biol. Rhythms* **23**, 26–36 (2008).
5. A. Z. Baburski, S. J. Sokanovic, M. M. Bjelic, S. M. Radovic, S. A. Andric, T. S. Kostic, Circadian rhythm of the Leydig cells endocrine function is attenuated during aging. *Exp. Gerontol.* **73**, 5–13 (2016).
6. T. Liu, W. He, Z. Zhong, C. Lu, L. Wu, Z. Wang, W. K. Smith, Q. Shi, Q. Long, H. Wang, The circadian clock orchestrates spermatogonial differentiation and fertilization by regulating retinoic acid signaling in vertebrates. *Natl. Sci. Rev.* **12**, nwae456 (2025).
7. T. Krieger, B. D. Simons, Dynamic stem cell heterogeneity. *Development* **142**, 1396–1406 (2015).
8. D. G. de Rooij, The nature and dynamics of spermatogonial stem cells. *Development* **144**, 3022–3030 (2017).
9. E. L. Bittman, Timing in the testis. *J. Biol. Rhythms* **31**, 12–36 (2016).
10. C. Han, Gene expression programs in mammalian spermatogenesis. *Development* **151**, dev202033 (2024).
11. M. Rabbani, X. Zheng, G. L. Manske, A. Vargo, A. N. Shami, J. Z. Li, S. S. Hammoud, Decoding the spermatogenesis program: New insights from transcriptomic analyses. *Annu. Rev. Genet.* **56**, 339–368 (2022).
12. D. F. Carrageta, S. C. Pereira, R. Ferreira, M. P. Monteiro, P. F. Oliveira, M. G. Alves, Signatures of metabolic diseases on spermatogenesis and testicular metabolism. *Nat. Rev. Urol.* **21**, 477–494 (2024).
13. L. J. Greenspan, M. de Cuevas, E. Matunis, Genetics of gonadal stem cell renewal. *Annu. Rev. Cell Dev. Biol.* **31**, 291–315 (2015).
14. T. Lord, B. Nixon, Metabolic changes accompanying spermatogonial stem cell differentiation. *Dev. Cell* **52**, 399–411 (2020).
15. R. Bose, G. Manku, M. Culty, S. S. Wing, Ubiquitin-proteasome system in spermatogenesis. *Adv. Exp. Med. Biol.* **759**, 181–213 (2014).
16. M. Kaneko, G. M. Cahill, Light-dependent development of circadian gene expression in transgenic zebrafish. *PLOS Biol.* **3**, e34 (2005).
17. N. Zhang, Y. Wang, Z. Chen, J. Ren, A. Rehman, D. W. Ahmad, D. Long, J. Hou, Y. Zhou, L. Yang, Y. Ni, Y. Li, C. Du, Y. Yu, M. Liao, Single-cell transcriptome analysis of Bisphenol A exposure reveals the key roles of the testicular microenvironment in male reproduction. *Biomed. Pharmacother.* **145**, 112449 (2022).
18. F. Dong, P. Ping, Y. Ma, X. F. Chen, Application of single-cell RNA sequencing on human testicular samples: A comprehensive review. *Int. J. Biol. Sci.* **19**, 2167–2197 (2023).
19. S. Lukassen, E. Bosch, A. B. Ekici, A. Winterpacht, Characterization of germ cell differentiation in the male mouse through single-cell RNA sequencing. *Sci. Rep.* **8**, 6521 (2018).
20. C. D. Green, Q. Ma, G. L. Manske, A. N. Shami, X. Zheng, S. Marini, L. Moritz, C. Sultan, S. J. Gurczynski, B. B. Moore, M. D. Tallquist, J. Z. Li, S. S. Hammoud, A comprehensive roadmap of murine spermatogenesis defined by single-cell RNA-seq. *Dev. Cell* **46**, 651–667.e10 (2018).
21. P. Qian, J. Kang, D. Liu, G. Xie, Single cell transcriptome sequencing of Zebrafish testis revealed novel spermatogenesis marker genes and stronger leydig-germ cell paracrine interactions. *Front. Genet.* **13**, 851719 (2022).
22. L. S. Mure, H. D. Le, G. Benegiamo, M. W. Chang, L. Rios, N. Jillani, M. Ngotho, T. Kariuki, O. Dkhissi-Benyahya, H. M. Cooper, S. Panda, Diurnal transcriptome atlas of a primate across major neural and peripheral tissues. *Science* **359**, eaao0318 (2018).
23. L. Li, J. Dong, L. Yan, J. Yong, X. Liu, Y. Hu, X. Fan, X. Wu, H. Guo, X. Wang, X. Zhu, R. Li, J. Yan, Y. Wei, Y. Zhao, W. Wang, Y. Ren, P. Yuan, Z. Yan, B. Hu, F. Guo, L. Wen, F. Tang, J. Qiao, Single-cell RNA-seq analysis maps development of human germline cells and gonadal niche interactions. *Cell Stem Cell* **20**, 891–892 (2017).
24. D. Crespo, L. H. C. Assis, H. J. G. van de Kant, S. de Waard, D. Safian, M. S. Lemos, J. Bogerd, R. W. Schulz, Endocrine and local signaling interact to regulate spermatogenesis in zebrafish: Follicle-stimulating hormone, retinoic acid and androgens. *Development* **146**, dev178665 (2019).
25. D. Morse, N. Cermakian, S. Brancorsini, M. Parvinen, P. Sassone-Corsi, No circadian rhythms in testis: Period1 expression is clock independent and developmentally regulated in the mouse. *Mol. Endocrinol.* **17**, 141–151 (2003).
26. C. Y. Cheng, D. D. Mruk, Cell junction dynamics in the testis: Sertoli-germ cell interactions and male contraceptive development. *Physiol. Rev.* **82**, 825–874 (2002).
27. P. T. Saunders, Germ cell-somatic cell interactions during spermatogenesis. *Reproduction* **61**, 91–101 (2003).
28. M. Chodkowski, A. Zielezinski, S. Anbalagan, A ligand-receptor interactome atlas of the zebrafish. *iScience* **26**, 107309 (2023).
29. S. Jin, C. F. Guerrero-Juarez, L. Zhang, I. Chang, R. Ramos, C. H. Kuan, P. Myung, M. V. Plikus, Q. Nie, Inference and analysis of cell-cell communication using CellChat. *Nat. Commun.* **12**, 1088 (2021).
30. L. O'Donnell, L. B. Smith, D. Rebourcet, Sertoli cells as key drivers of testis function. *Semin. Cell Dev. Biol.* **121**, 2–9 (2022).
31. L. Zhao, C. Yao, X. Xing, T. Jing, P. Li, Z. Zhu, C. Yang, J. Zhai, R. Tian, H. Chen, J. Luo, N. Liu, Z. Deng, X. Lin, N. Li, J. Fang, J. Sun, C. Wang, Z. Zhou, Z. Li, Single-cell analysis of developing and azoospermia human testicles reveals central role of Sertoli cells. *Nat. Commun.* **11**, 5683 (2020).
32. M. D. Griswold, Spermatogenesis: The commitment to meiosis. *Physiol. Rev.* **96**, 1–17 (2016).
33. L. Li, B. Yan, Y. Q. Shi, W. Q. Zhang, Z. L. Wen, Live imaging reveals differing roles of macrophages and neutrophils during zebrafish tail fin regeneration. *J. Biol. Chem.* **287**, 25353–25360 (2012).
34. D. M. Leerberg, K. Sano, B. W. Draper, Fibroblast growth factor signaling is required for early somatic gonad development in zebrafish. *PLOS Genet.* **13**, e1006993 (2017).
35. A. Griffin, S. Parajes, M. Weger, A. Zaucker, A. E. Taylor, D. M. O'Neil, F. Muller, N. Krone, Ferredoxin 1b (Fdx1b) is the essential mitochondrial redox partner for cortisol biosynthesis in zebrafish. *Endocrinology* **157**, 1122–1134 (2016).
36. L. J. Martin, F. Bergeron, R. S. Viger, J. J. Tremblay, Functional cooperation between GATA factors and cJUN on the star promoter in MA-10 Leydig cells. *J. Androl.* **33**, 81–87 (2012).
37. P. R. Manna, D. M. Stocco, Crosstalk of CREB and Fos/Jun on a single cis-element: Transcriptional repression of the steroidogenic acute regulatory protein gene. *J. Mol. Endocrinol.* **39**, 261–277 (2007).
38. R. Medicherla, S. Leers-Sucheta, Y. Luo, S. Azhar, Impaired activation of AP-1 and altered expression of constituent proteins in rat adrenal during ageing. *Mech. Ageing Dev.* **122**, 1169–1186 (2001).
39. S. Jenab, P. L. Morris, Testicular leukemia inhibitory factor (LIF) and LIF receptor mediate phosphorylation of signal transducers and activators of transcription (STAT)-3 and STAT-1 and induce c-fos transcription and activator protein-1 activation in rat Sertoli but not germ cells. *Endocrinology* **139**, 1883–1890 (1998).
40. T. DeFalco, S. J. Potter, A. V. Williams, B. Waller, M. J. Kan, B. Capel, Macrophages contribute to the spermatogonial niche in the adult testis. *Cell Rep.* **12**, 1107–1119 (2015).
41. C. Trapnell, D. Cacchiarelli, J. Grimsby, P. Pokharel, S. Li, M. Morse, N. J. Lennon, K. J. Livak, T. S. Mikkelsen, J. L. Rinn, The dynamics and regulators of cell fate decisions are revealed by pseudotemporal ordering of single cells. *Nat. Biotechnol.* **32**, 381–386 (2014).
42. X. Qiu, Q. Mao, Y. Tang, L. Wang, R. Chawla, H. A. Pliner, C. Trapnell, Reversed graph embedding resolves complex single-cell trajectories. *Nat. Methods* **14**, 979–982 (2017).
43. M. C. Leal, E. R. Cardoso, R. H. Nobrega, S. R. Batlouni, J. Bogerd, L. R. Franca, R. W. Schulz, Histological and stereological evaluation of zebrafish (*Danio rerio*) spermatogenesis with an emphasis on spermatogonial generations. *Biol. Reprod.* **81**, 177–187 (2009).
44. Q. Lin, J. Mei, Z. Li, X. Zhang, L. Zhou, J. F. Gui, Distinct and cooperative roles of amh and dmrt1 in self-renewal and differentiation of male germ cells in zebrafish. *Genetics* **207**, 1007–1022 (2017).
45. L. Zhou, Y. Feng, F. Wang, X. Dong, L. Jiang, C. Liu, Q. Zhao, K. Li, Generation of all-male-like sterile zebrafish by eliminating primordial germ cells at early development. *Sci. Rep.* **8**, 1834 (2018).
46. A. N. Shami, X. Zheng, S. K. Munyoki, Q. Ma, G. L. Manske, C. D. Green, M. Sukhwani, K. E. Orwig, J. Z. Li, S. S. Hammoud, Single-cell RNA sequencing of human, macaque, and mouse testes uncovers conserved and divergent features of mammalian spermatogenesis. *Dev. Cell* **54**, 529–547.e12 (2020).
47. C. M. Smendziuk, A. Messenberg, A. W. Vogl, G. Tanentzapf, Bi-directional gap junction-mediated soma-germline communication is essential for spermatogenesis. *Development* **142**, 2598–2609 (2015).
48. K. L. Lu, Y. M. Yamashita, Germ cell connectivity enhances cell death in response to DNA damage in the *Drosophila* testis. *eLife* **6**, e27960 (2017).
49. M. P. Greenbaum, W. Yan, M. H. Wu, Y. N. Lin, J. E. Agno, M. Sharma, R. E. Braun, A. Rajkovic, M. M. Matzuk, TEX14 is essential for intercellular bridges and fertility in male mice. *Proc. Natl. Acad. Sci. U.S.A.* **103**, 4982–4987 (2006).
50. K. F. Rodriguez, P. R. Brown, C. M. Amato, B. Nicol, C.-F. Liu, X. Xu, H. H.-C. Yao, Somatic cell fate maintenance in mouse fetal testes via autocrine/paracrine action of AMH and activin B. *Nat. Commun.* **13**, 4130 (2022).
51. S. Di Persio, T. Tekath, L. M. Siebert-Kuss, J.-F. Cremers, J. Wistuba, X. Li, G. Meyer Zu Hörste, H. C. A. Drexler, M. J. Wyrwoll, F. Tüttelmann, M. Dugas, S. Kliesch, S. Schlatt, S. Laurentino, N. Neuhaus, Single-cell RNA-seq unravels alterations of the human spermatogonial stem cell compartment in patients with impaired spermatogenesis. *Cell Rep. Med.* **2**, 100395 (2021).
52. M. Inaba, M. Buszczak, Y. M. Yamashita, Nanotubes mediate niche-stem-cell signalling in the Drosophila testis. *Nature* **523**, 329–332 (2015).
53. S. Ladyzhets, M. Antel, T. Simao, N. Gasek, A. E. Cowan, M. Inaba, Self-limiting stem-cell niche signaling through degradation of a stem-cell receptor. *PLOS Biol.* **18**, e3001003 (2020).

54. D. D. Mruk, C. Y. Cheng, The mammalian blood-testis barrier: Its biology and regulation. *Endocr. Rev.* **36**, 564–591 (2015).
55. J. Chen, X. Yang, M. Cui, Z. Yao, Z. Ouyang, Z. Qu, Y. Huang, Y. Zhu, J. Zhao, G. Chang, Deciphering the regulatory networks of human male germline development from embryo to adulthood. *Biochim. Biophys. Acta Mol. Basis Dis.* **1871**, 167918 (2025).
56. Q. Liu, M. Yu, Z. Lin, L. Wu, P. Xia, M. Zhu, B. Huang, W. Wu, R. Zhang, K. Li, L. Zhu, Q. Wang, COL1A1-positive endothelial cells promote gastric cancer progression via the ANGPTL4-SDC4 axis driven by endothelial-to-mesenchymal transition. *Cancer Lett.* **623**, 217731 (2025).
57. J. Kalucka, L. P. M. H. de Rooij, J. Goveia, K. Rohlenova, S. J. Dumas, E. Meta, N. V. Conchinha, F. Taverna, L. A. Teuwen, K. Veys, M. Garcia-Caballero, S. Khan, V. Geldhof, L. Sokol, R. Chen, L. Treps, M. Borri, P. de Zeeuw, C. Dubois, T. K. Karakach, K. D. Falkenberg, M. Parys, X. Yin, S. Vinckier, Y. Du, R. A. Fenton, L. Schoonjans, M. Dewerchin, G. Eelen, B. Thienpont, L. Lin, L. Bolund, X. Li, Y. Luo, P. Carmeliet, Single-cell transcriptome atlas of murine endothelial cells. *Cell* **180**, 764–779.e20 (2020).
58. J. Taelman, S. M. Czukiewska, I. Moustakas, Y. W. Chang, S. Hillenius, T. van der Helm, L. E. van der Meeren, H. Mei, X. Fan, S. M. Chuva de Sousa Lopes, Characterization of the human fetal gonad and reproductive tract by single-cell transcriptomics. *Dev. Cell* **59**, 529–544.e5 (2024).
59. X.-W. Yu, T.-T. Li, X.-M. Du, Q.-Y. Shen, M.-F. Zhang, Y.-D. Wei, D.-H. Yang, W.-J. Xu, W.-B. Chen, C.-L. Bai, X.-L. Li, G.-P. Li, N. Li, S. Peng, M.-Z. Liao, J.-L. Hua, Single-cell RNA sequencing reveals atlas of dairy goat testis cells. *Zool. Res.* **42**, 401–405 (2021).
60. M. R. Elliott, S. Zheng, D. Park, R. I. Woodson, M. A. Reardon, I. J. Juncadella, J. M. Kinchen, J. Zhang, J. J. Lysiak, K. S. Ravichandran, Unexpected requirement for ELMO1 in clearance of apoptotic germ cells in vivo. *Nature* **467**, 333–337 (2010).
61. L. J. Martin, H. T. Nguyen, Basic leucine zipper transcription factors as important regulators of leydig cells' functions. *Int. J. Mol. Sci.* **23**, 12887 (2022).
62. H. T. Nguyen, M. Najih, L. J. Martin, The AP-1 family of transcription factors are important regulators of gene expression within Leydig cells. *Endocrine* **74**, 498–507 (2021).
63. H. S. Abdou, N. M. Robert, J. J. Tremblay, Calcium-dependent Nr4a1 expression in mouse Leydig cells requires distinct AP1/CRE and MEF2 elements. *J. Mol. Endocrinol.* **56**, 151–161 (2016).
64. J. Gibbs, L. Ince, L. Matthews, J. Mei, T. Bell, N. Yang, B. Saer, N. Begley, T. Poolman, M. Pariollaud, S. Farrow, F. DeMayo, T. Hussell, G. S. Worthen, D. Ray, A. Loudon, An epithelial circadian clock controls pulmonary inflammation and glucocorticoid action. *Nat. Med.* **20**, 919–926 (2014).
65. D. Tang, R. Kang, H. J. Zeh, M. T. Lotze, The multifunctional protein HMGB1: 50 years of discovery. *Nat. Rev. Immunol.* **23**, 824–841 (2023).
66. L. Y. Du, P. Keerthisinghe, L. Rolland, Y. J. Sung, H. Darroch, T. Linnerz, E. Ashimbayeva, M. J. Grant, P. M. Kakadia, A. Ramachandran, A. Tups, H. P. Spaink, S. K. Bohlander, J. Cheeseman, P. S. Crosier, J. W. Astin, G. Warman, C. J. Hall, A light-regulated circadian timer optimizes neutrophil bactericidal activity to boost daytime immunity. *Sci. Immunol.* **10**, eadn3080 (2025).
67. N. Trost, N. Mbengue, H. Kaessmann, The molecular evolution of mammalian spermatogenesis. *Cells Dev.* **175**, 203865 (2023).
68. M. Chen, N. Wang, H. Yang, D. Liu, Y. Gao, L. Duo, X. Cui, F. Hao, J. Ye, F. Gao, Q. Tu, Y. Gui, Single-cell transcriptome analysis of the germ cells and somatic cells during mitotic quiescence stage in goats. *FASEB J.* **37**, e23244 (2023).
69. B. Suresh, J. Lee, S.-H. Hong, K.-S. Kim, S. Ramakrishna, The role of deubiquitinating enzymes in spermatogenesis. *Cell. Mol. Life Sci.* **72**, 4711–4720 (2015).
70. M. Westerfield, *The Zebrafish Book. A Guide for the Laboratory Use of Zebrafish (Danio rerio)* (University of Oregon Press, ed. 5, 2007).
71. Y. Hao, S. Hao, E. Andersen-Nissen, W. M. Mauck III, S. Zheng, A. Butler, M. J. Lee, A. J. Wilk, C. Darby, M. Zager, P. Hoffman, M. Stoeckius, E. Papalexi, E. P. Mimitou, J. Jain, A. Srivastava, T. Stuart, L. M. Fleming, B. Yeung, A. J. Rogers, J. M. McElrath, C. A. Blish, R. Gottardo, P. Smibert, R. Satija, Integrated analysis of multimodal single-cell data. *Cell* **184**, 3573–3587.e29 (2021).
72. G. Huang, F. Zhang, Q. Ye, H. Wang, The circadian clock regulates autophagy directly through the nuclear hormone receptor Nr1d1/Rev-erbα and indirectly via Cebpb/(C/ebpβ) in zebrafish. *Autophagy* **12**, 1292–1309 (2016).
73. J. Dopp, A. Ortega, K. Davie, S. Poovathingal, E. S. Baz, S. Liu, Single-cell transcriptomics reveals that glial cells integrate homeostatic and circadian processes to drive sleep-wake cycles. *Nat. Neurosci.* **27**, 359–372 (2024).
74. C. Trapnell, A. Roberts, L. Goff, G. Pertea, D. Kim, D. R. Kelley, H. Pimentel, S. L. Salzberg, J. L. Rinn, L. Pachter, Differential gene and transcript expression analysis of RNA-seq experiments with TopHat and Cufflinks. *Nat. Protoc.* **7**, 562–578 (2012).
75. S. Zhang, M. Xu, J. Huang, L. Tang, Y. Zhang, J. Wu, S. Lin, H. Wang, Heme acts through the Bach1b/Nrf2a-MafK pathway to regulate exocrine peptidase precursor genes in porphyric zebrafish. *Dis. Model. Mech.* **7**, 837–845 (2014).
76. O. Fornes, J. A. Castro-Mondragon, A. Khan, R. van der Lee, X. Zhang, P. A. Richmond, B. P. Modi, S. Correard, M. Gheorghe, D. Baranasic, W. Santana-Garcia, G. Tan, J. Cheneby, B. Ballester, F. Parcy, A. Sandelin, B. Lenhard, W. W. Wasserman, A. Mathelier, JASPAR 2020: Update of the open-access database of transcription factor binding profiles. *Nucleic Acids Res.* **48**, D87–D92 (2020).
77. M. Wang, Z. Zhong, Y. Zhong, W. Zhang, H. Wang, The zebrafish period2 protein positively regulates the circadian clock through mediation of retinoic acid receptor (RAR)-related orphan receptor α (Rorα). *J. Biol. Chem.* **290**, 4367–4382 (2015).
78. L. Wu, M. Zhao, X. Chen, H. Wang, A *miR-219-5p-bmal1b* negative feedback loop contributes to circadian regulation in zebrafish. *Commun. Biol.* **7**, 1671 (2024).
79. S. K. Mishra, T. Liu, H. Wang, Thousands of oscillating LncRNAs in the mouse testis. *Comput. Struct. Biotechnol. J.* **23**, 330–346 (2024).
80. S. K. Mishra, Z. Zhong, H. Wang, Hundreds of LncRNAs display circadian rhythmicity in zebrafish larvae. *Cells* **10**, 3173 (2021).
81. H. R. Ueda, S. Hayashi, W. Chen, M. Sano, M. Machida, Y. Shigeyoshi, M. Iino, S. Hashimoto, System-level identification of transcriptional circuits underlying mammalian circadian clocks. *Nat. Genet.* **37**, 187–192 (2005).
82. C. E. Grant, T. L. Bailey, W. S. Noble, FIMO: Scanning for occurrences of a given motif. *Bioinformatics* **27**, 1017–1018 (2011).

Acknowledgments: We thank the members of the Wang Lab for discussions and Z. Zhong and J. Hu for technical support. **Funding:** This study was supported by grants from the National Key R&D Program of China (2019YFA0802400) (H.W.), the National Natural Science Foundation of China (NSFC) (#32571347, #81701347, #31961133026, #81570171, and #31871187) (H.W.), the Priority Academic Program Development (PAPD) of Jiangsu Higher Education Institutions, and the Natural Science Foundation of Jiangsu Province (no. BK20255001). **Author contributions:** T.L.: Writing—original draft, conceptualization, investigation, writing—review and editing, methodology, data curation, validation, formal analysis, software, and visualization. L.W.: Investigation. S.K.M.: Investigation, writing—review and editing, and formal analysis. Q.F.: Investigation. H.W.: Writing—original draft, conceptualization, investigation, writing—review and editing, methodology, resources, funding acquisition, data curation, validation, supervision, formal analysis, and project administration. **Competing interests:** The authors declare that they have no competing interests. **Data, code, and materials availability:** All data and code needed to evaluate and reproduce the results in the paper are present in the paper and/or the Supplementary Materials. The raw data from time-series bulk RNA-seq and scRNA-seq have been deposited in the NCBI database under accession numbers PRJNA579855 and GSE206024, respectively. The materials generated in this study, such as plasmids, are available from H.W. (Email: han.wang88@gmail.com or wanghan@suda.edu.cn) upon request. Material distribution will comply with standard institutional material transfer agreements (MTA).

Submitted 12 December 2025
Accepted 1 May 2026
Published 12 June 2026
10.1126/sciadv.aee7124